Marine Geology 480 (2025) 107447

Contents lists available at ScienceDirect

Marine Geology

journal homepage: www.elsevier.com/locate/margo

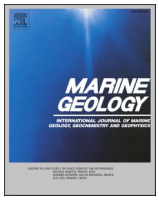

Impact of Paleocene–Eocene tectonic and climatic forcing on Arctic sediment transfer variability: SW Barents Sea, Norway

Amando P.E. Lasabuda [a,b,c,d,*], Domenico Chiarella [b,e], Tor Oftedal Sømme [f], Sten-Andreas Grundvåg [a], Isak Eikelmann [a], Stig-Morten Knutsen [g], Anthony George Doré [h], Jan Sverre Laberg [a], Tom Arne Rydningen [a], Alfred Hanssen [a], Bent Kjølhamar [i]

[a] Department of Geosciences, UiT The Arctic University of Norway, Tromsø, Norway
[b] Clastic Sedimentology Investigation (CSI), Department of Earth Sciences, Royal Holloway University of London, Egham, UK
[c] Centre for Planetary Habitability (PHAB), Department of Geosciences, University of Oslo, Oslo, Norway
[d] Earthbyte Group, School of Geosciences, The University of Sydney, Sydney, Australia
[e] Biological, Geological and Environmental Sciences Department, Alma Mater Studiorum University of Bologna, Bologna, Italy
[f] Equinor ASA, Fornebu, Norway
[g] The Norwegian Offshore Directorate, Harstad, Norway
[h] Energy and Geoscience Institute (EGI), The University of Utah, Salt Lake City, USA
[i] TGS, Oslo, Norway

ARTICLE INFO

Editor: Michele Rebesco

Keywords:
Arctic
Sediment
Source-to-sink
Climate
Tectonic

ABSTRACT

During the Paleocene and Eocene, many Arctic basins experienced multiple, yet synchronous periods of increased sedimentation rates. Several causal factors have been suggested including major volcanic events, tectonic plate reorganization and plate break-up, as well as widespread uplift along with contemporaneous and short-lived hyperthermal events. However, the significance of and relation between tectonic and climatic forcing on Arctic sediment transfer during the early Paleogene are poorly understood. In this case study from the Barents Shelf margin in the Norwegian Arctic, we present previously unpublished cores combined with exploration wells, and new high-resolution 3D seismic data to investigate sedimentary stacking patterns and geomorphological features in the Sørvestsnaget Basin. Our integrated investigations reveal the development of climate-controlled and tectonically-driven submarine fans. The PETM fans display an individual fan as a result of single depositional event compared to the middle Eocene fans that show stacked submarine fans probably deposited during multi-phase events. Our stratigraphic forward modelling analysis indicates that regional-scale tectonically induced uplift significantly increased the amount of sand delivered to the basin as documented by a thickening of the basin fill succession. The climatic component contributes to sand transport variability to the basin, and thus the temporal evolution pattern of sand is much varied. Finally, we discuss our findings with the tectonic and climatic forcing factors in a circum-Arctic perspective.

1. Introduction

The Paleocene and Eocene epochs are characterised by a series of hyperthermal events (Zachos et al., 2001; Röhl et al., 2007) and elevated CO_2 levels in the atmosphere (Zachos et al., 2008; Westerhold et al., 2020). Across the Arctic and North Atlantic regions, these events have been variably linked to plate breakup and seafloor spreading associated with the opening of the North Atlantic and its northward propagation (Faleide et al., 2015; Doré et al., 2016), major volcanic events related to the emplacement of the North Atlantic Igneous Province (Svensen et al., 2004; Wilkinson et al., 2017) and widespread thermal/tectonic uplift associated with mantle plume dynamics (Japsen and Chalmers, 2000; Lasabuda et al., 2021). However, the intricate relationship between the regional tectonics and the extreme climate perturbations during the Paleocene–Eocene, and their combined impact on the sediment flux to basins situated along the margins of the North Atlantic Ocean is not well understood, particularly for its Arctic segment.

The hyperthermal events, such as the Paleocene–Eocene Thermal Maximum (PETM, c. 55.9 Ma) may provide analogues and projections to future climatic conditions if global warming continues (Zachos et al.,

* Corresponding author at: Department of Geosciences, UiT The Arctic University of Norway, Tromsø, Norway.
E-mail address: ado.amando@gmail.com (A.P.E. Lasabuda).

https://doi.org/10.1016/j.margeo.2024.107447
Received 13 June 2024; Received in revised form 20 November 2024; Accepted 25 November 2024
Available online 29 November 2024

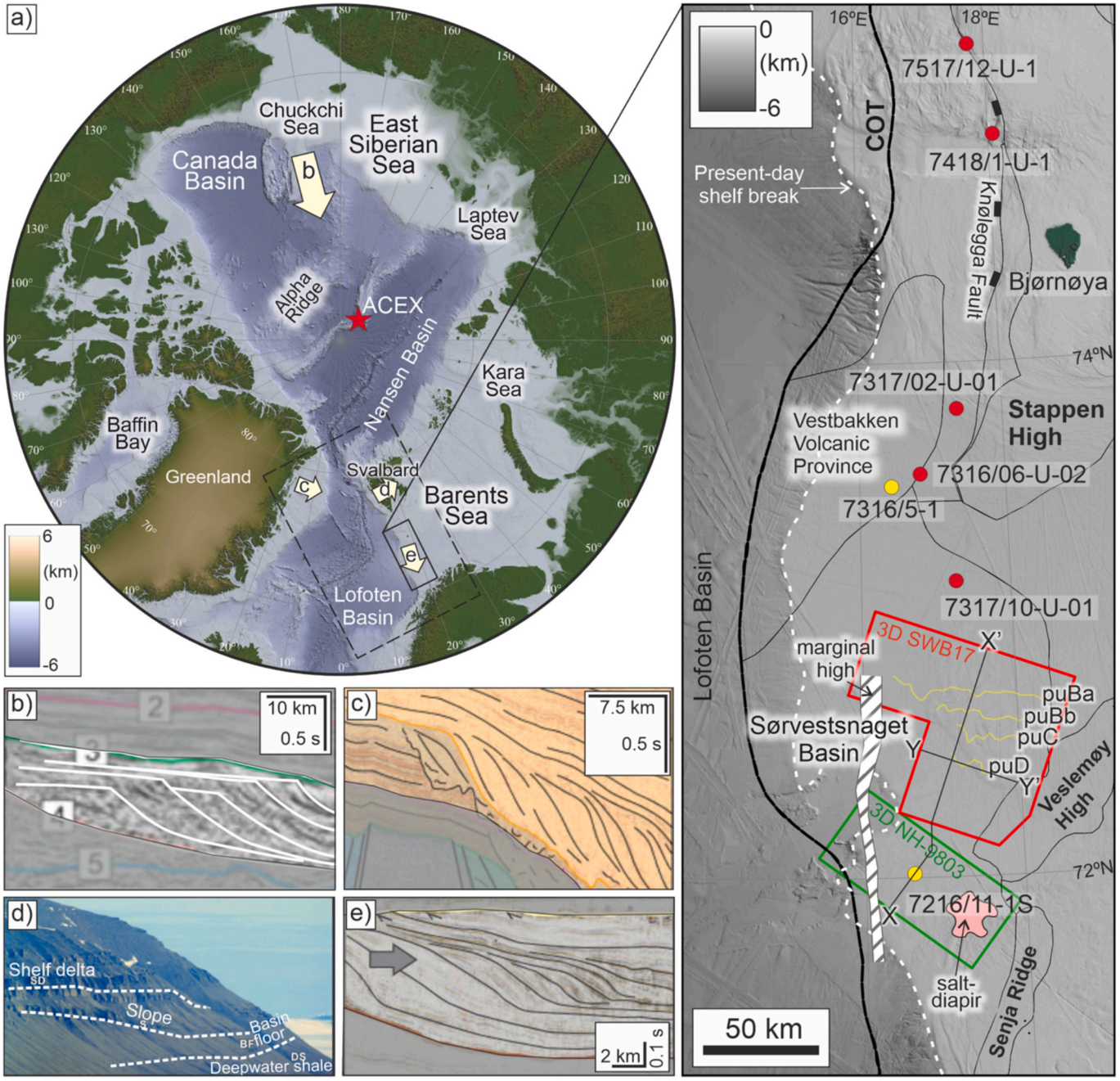

Fig. 1. The Barents Sea in the circum-Arctic framework. a) Present-day structural elements in the Arctic including highs, shelves and basins relevant for this study. The position of the ACEX is shown by a red star, and the direction of Eocene sediment progradation is indicated by arrows. The dashed black rectangle is the location of reconstructed plate tectonics in Fig. 2. The inset map shows the location of well data (yellow circle), boreholes (red circle) and 3D seismic data cubes (SWB17 in red line and NH-9803 in green line). The location of representative seismic profiles X-X' and Y-Y′ as shown in Fig. 6 are indicated (note that seismic profile *Z*-Z' is the zoom-in version of profile Y-Y′ and therefore, is not shown here). The bold line in the inset map represents the COT – Continental to Ocean Transition (Gabrielsen et al., 1990), while the white dashed line represents the present-day shelf break. Bathymetry is adapted from GEBCO (2022). The structural elements are taken from the Norwegian Offshore Directorate (Gabrielsen et al., 1990). The mapped shelf edges for prograding unit puBa, puBb, puC and puD (sensu Safronova et al., 2014) are shown as yellow lines. Examples of Eocene clinoform systems that have been reported in the Arctic, such as b) the Chukchi region (Hegewald and Jokat, 2013), c) the Thetis Basin, offshore Greenland (Hovikoski et al., 2021; Petersen, 2021), d) the Central Tertiary Basin, Spitsbergen (Helland-Hansen and Grundvåg, 2021), and e) the Sørvestsnaget Basin, SW Barents Sea (Safronova et al., 2014; Lasabuda et al., 2018a). (For interpretation of the references to colour in this figure legend, the reader is referred to the web version of this article.)

2001; Röhl et al., 2007; Svensen et al., 2019; Westerhold et al., 2020). After the PETM, there are two other hyperthermal events within the Early Eocene Climate Optimum (EECO), namely the Eocene Thermal Maxima 2 and 3 (ETM-2 at c. 53.5, and ETM-3 at c. 53.16) (Sluijs et al., 2009; Stap et al., 2010; Thomas et al., 2018; Westerhold et al., 2018). However, the EECO is a relatively long period (> 2 Myrs) of sustained warm temperatures and is not considered hyperthermal, which is short-lived (<200 to 300 kyrs) (Westerhold et al., 2007; Zachos et al., 2008). In addition to the relatively synchronous tectonism recorded across the region during the Paleocene–Eocene (Green and Duddy, 2010), several Arctic basins, including the Barents Shelf, acted as major depositional sinks for sediments derived from uplifted and exposed terrains, as

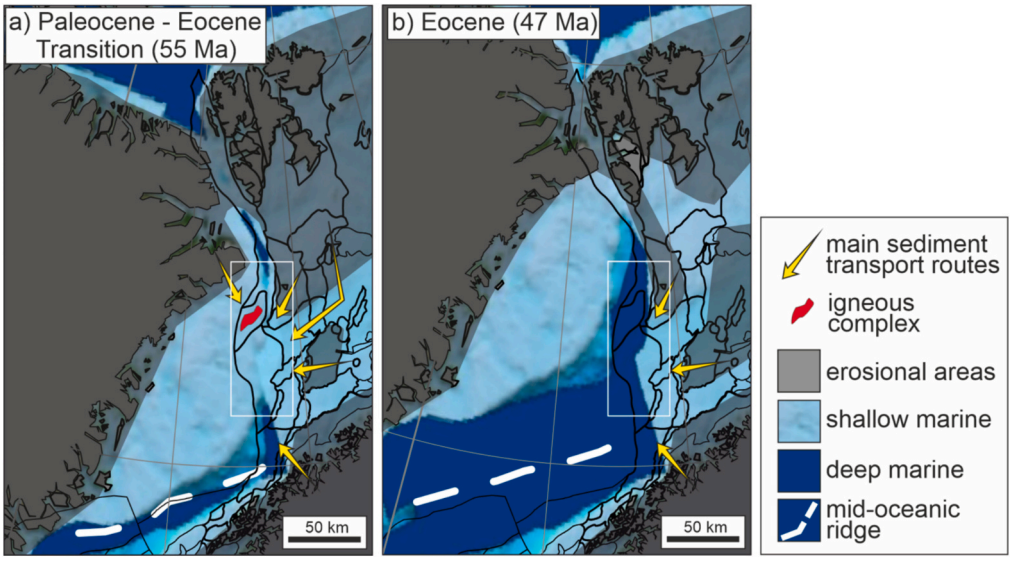

Fig. 2. Plate reconstructions of the NE Atlantic. a) Plate reconstruction during continental breakup (c. 55 Ma) that largely coincides with Paleocene–Eocene Thermal Maximum (PETM) at c. 55.9 Ma. The red area represents the igneous complex found in the Vestbakken Volcanic Province (Faleide et al., 1993; Omosanya et al., 2016). b) Plate configuration during the middle Eocene (47 Ma). The reconstructions are based on GPlates v.2.3 (Müller et al., 2019). The erosional areas follow Smelror et al. (2009) and Lasabuda et al. (2018a). Structural elements are taken from the Norwegian Offshore Directorate (Gabrielsen et al., 1990). The study area is shown as a white rectangle.

evidenced by a number of time-equivalent prograding sedimentary wedges (i.e., clinoform systems) and submarine fans widely occurring across the Arctic (Fig. 1a–e) (Hegewald and Jokat, 2013; Safronova et al., 2014; Lasabuda et al., 2018a; Helland-Hansen and Grundvåg, 2021; Hovikoski et al., 2021; Petersen, 2021). These depositional systems thus provide unique proxies to investigate the sedimentary response of Arctic sediments to the Paleocene–Eocene tectonic and climatic forcing.

Following the NE Atlantic breakup (c. 55 Ma), the SW Barents Sea margin, particularly in the Vestbakken Volcanic Province experienced basin formation and volcanic events, (Figs. 1a and 2a; Faleide et al., 2015; Doré et al., 2016). Volcanism may have contributed to the early phase of uplift around the Stappen high area, which was associated with plate break-up and sea-floor spreading (Faleide et al., 1993; Lasabuda et al., 2021). In the middle Eocene (c. 47 Ma), the sediment flux to the marginal basins increased drastically, amongst others recorded by southward-prograding clinothems (i.e., clinoform-bounded sedimentary units) in the Sørvestsnaget Basin evidently sourced from the uplifted Stappen High (Safronova et al., 2014). Similar-scaled clinoforms of inferred early to middle Eocene age also present in the Central Tertiary Basin (CTB) of Spitsbergen sourced from a local fold-and-thrust belt that formed in response to the Eurekan compression (Figs. 1d, e and 2b; Piepjohn et al., 2016; Helland-Hansen and Grundvåg, 2021).

Previous mapping efforts in the circum-Arctic utilised mainly 2D seismic data (e.g., Hegewald and Jokat, 2013; Hovikoski et al., 2021; Petersen, 2021), limited boreholes such as ACEX – Arctic Coring Expedition (Moran et al., 2006; Backman et al., 2008) and outcrop studies on Svalbard (e.g., Helland-Hansen and Grundvåg, 2021), northern Greenland (e.g., Lyck and Stemmerik, 2000) and the Canadian Arctic (e.g., Ricketts and Stephenson, 1994; Mosher et al., 2012; Coakley et al., 2016; Evangelatos and Mosher, 2016). Conversely, the Norwegian Barents Shelf is widely covered by scientific shallow boreholes, deep exploration wells and high-resolution 2D—3D seismic data due to resources-related commercial activity and research and development projects. When integrated, these subsurface data can bridge the gap between local, detailed stratigraphic mapping on cores and the large, basin-scale perspective needed to capture the dynamics of a source-to-sink system under variable tectonic and climatic perturbations, particularly in a frontier area in the Arctic where data are limited.

Paleocene–Eocene tectonic uplift and climatic events are responsible for the geomorphology of the SW Barents Sea basin and associated basin-fill stratigraphy. We aim to test this hypothesis through analysis of new 3D seismic data, shallow stratigraphic boreholes and industry exploration well information. The influence of tectonic events and climatic components on sediment transfer to the basins is simulated using stratigraphic forward modelling techniques. However, note that we do not attempt to precisely separate between tectonic and climatic signals due to the limitation of chronological constraints in our stratigraphic record, particularly the ETM during EECO, which is also below our seismic data resolution. Nevertheless, We show that the short-lived hyperthermal event of PETM has contributed to the sedimentation pattern dynamics, where long-lived tectonic uplift has played a major role in controlling the sediment supply.

2. Materials and methods

We used core data from both shallow stratigraphic drillings and exploration wells. The term shallow borehole used here represents a shallow sedimentary core which was drilled less than 600 m. This shallow borehole is different from wells drilled for hydrocarbon exploration purposes, which are typically down to thousands of meters. Well data include gamma-ray well-logs and a stratigraphic core and should not be confused with cores from shallow drillings/boreholes.

2.1. Shallow boreholes: core dating and description methodology

Shallow stratigraphic cores 7517/12-U-01 and 7418/01-U-01 were part of a drilling program in 1994 totaling nine boreholes at six different locations between Bjørnøya and Svalbard. Five borehole descriptions published by Sættem et al. (1994) and three of these, which contain Paleocene and Eocene strata are presented in Fig. 3. Key results from shallow cores 7517/12-U-01 and 7418/01-U-01 presented here were part of the MSc thesis of Eikelmann (2017). Borehole 7515/12-U-01 located at 75°14′16.4” N 17°44′59.2″ E was drilled at a water depth of 156 m. The total depth from the seabed was 200 m, and a total of 87.8 m of cores were collected. Borehole 7418/01-U-01 is located at 74°52′33.3” N 18°5′48.8″ E and was drilled at a water depth of 181.5 m. The total depth from the seabed was 126.15 m, and 113.3 m of cores

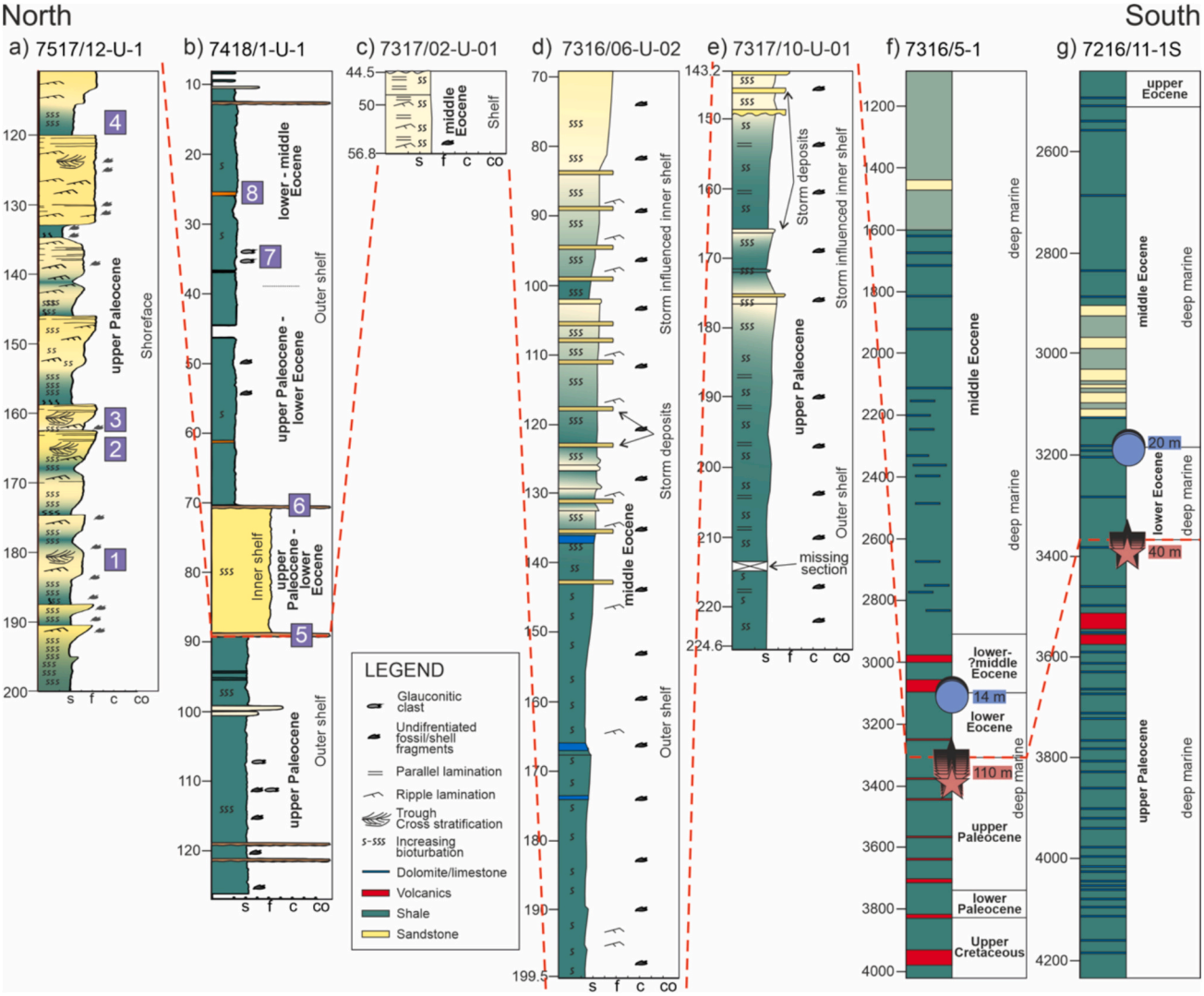

Fig. 3. Lithology from shallow cores and well data containing Paleocene–Eocene strata. Sedimentary logs of the shallow cores and our interpretation a) 7517/12-U-1; b) 7418/1-U-1; c) 7317/02-U-01; d) 7316/06-U-02; e) 7317/10-U-01. Cores c, d and e are redrawn by Sættem et al. (1994). The location of core photos (number 1–6 in purple rectangles) is shown in the core drawings (Supplementary Fig. 1). Lithological description of f) well 7316/5–1 in the Vestbakken Volcanic Province and g) well 7216/11-1S in the Sørvestsnaget Basin is indicated (Ryseth et al., 2003; Eidvin et al., 2022). The *Apectodinium Augustum* indicating the PETM event is shown as red-ish stars, recorded in a 110 m thick interval (levels 3410–3300 m) in well 7316/5–1 and in a 40 m thick interval (levels 3410–3370 m) in well 7216/11-1S. The *Azolla Acme* indicating the EECO is shown as blue circles, recorded in a 14 m thick interval (levels 3114–3100 m) in well 7316/5–1 and in a 20 m thick interval (levels 3190–3170 m) in well 7216/11-1S. See Fig. 1 for location. The red stippled line represents the base Eocene strata.

were collected. The cores were visually described based on lithology, grain size, colour, primary sedimentary structures, vertical continuity of beds (e.g., fault presence), nature of bed boundaries, stratigraphic contacts, and other secondary sedimentological features (e.g., bioturbations, concretions).

Biostratigraphic data were used to date the sedimentary strata in the studied boreholes. In borehole 7517/12-U-01, late Paleocene age is indicated for the strata between 200 and 110.75 m. In borehole 7418/01-U-01, biostratigraphic analysis shows *Reticulophragmium Pauperva* from 126.5 m to 89.9 m (late Paleocene), *Haplophragmoides Excavatus* from 89.9 m to 40 m (late Paleocene–early Eocene) and *Karrerulina Coniformis* from 35 m to 10 m (early–middle Eocene).

2.2. Exploration wells: core dating and well-logs analysis

Formation tops, chronology and well-log data were retrieved from the DISKOS database (https://www.sodir.no/en/diskos/). Biostratigraphic analysis was performed to identify the age and associated climatic events recorded in the stratigraphy (Equinor, 2023). *Apectodinium Augustum* and *Azolla Acme* (freshwater ferns) were used to identify the PETM and EECO events, respectively (Brinkhuis et al., 2006; Sluijs and Brinkhuis, 2009; Barke et al., 2012; Berndt et al., 2023). However, based on our current biostratigraphic data availability, we are not able to distinguish hyperthermal events around the EECO (i.e., ETM-2 and ETM-3), which require more species.

For well-log data, a gamma ray cut-off of 75 was selected to define the initial sandstone-shale boundary. Then, this lithological description was calibrated and corrected using completion reports of wells 7316/5–1 and 7216/11-1S (NPD, 2023).

2.3. Seismic data

The newer 3D seismic reflection data "SWB17" are owned by TGS and were acquired in 2011, 2012, and 2016 using ten and twelve 8 km long streamers and a dual source, 25 m long flip-flop. The data cover 14.150 km^2 with bin size 25 × 12.5 m. The data were processed and are

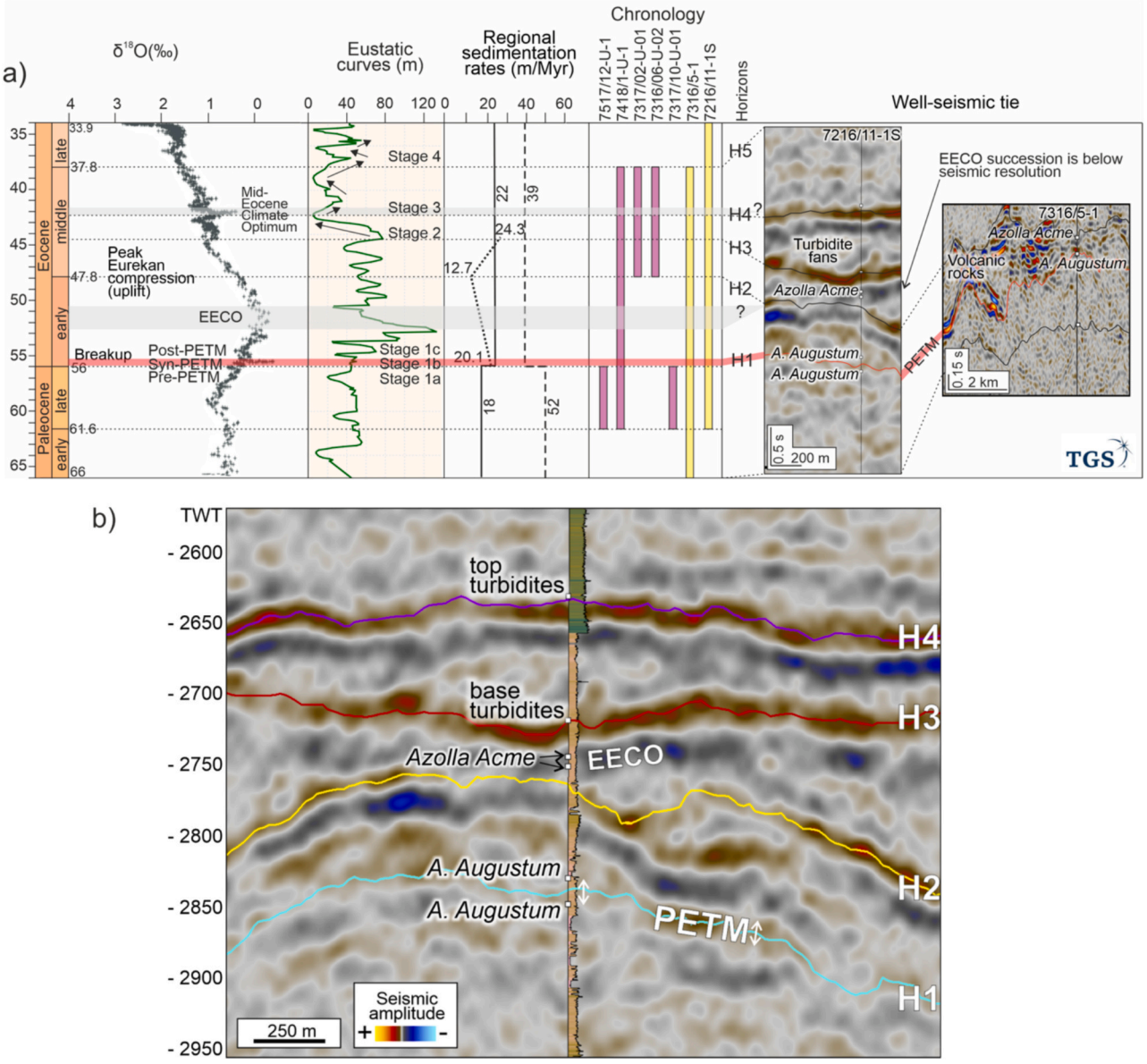

Fig. 4. a) Link between global climatic and regional tectonic events and local seismic geomorphological expressions. Isotope Oxygen and the corresponding climatic and tectonic events are adapted from Zachos et al. (2008). The global eustatic sea-level curve is taken from Miller et al. (2005). Correlations between sea-level fluctuation and key development stages from Fig. 10 are shown. Regional sedimentation rates are based on the ACEX result (dotted line) by Backman et al. (2008) and a volumetric mass balance study from the northwestern Barents Sea (dashed line) by Lasabuda et al. (2018b) and southwestern Barents Sea (continuous line) by Lasabuda et al. (2018a). Chronology of cores and well data presented in this study is indicated. Correlation of seismic horizons H1 – H4 to the key Paleocene–Eocene interval at well 7216/11-1S and 7316/5–1 are also shown. b) A zoom-in figure of a well-to-seismic tie at the location of well 7216/11-1S that is used for generating an RMS amplitude map for the PETM succession. Note the EECO layer is too thin and below seismic resolution in this study (see text for explanation/discussion).

characterised as PSTM (Post Stack Time Migration) cube. The older 3D seismic data NH-9803, south of SWB17, were acquired in 1998 by NorskHydro using eight 4050 m long streamers and dual sources. The NH9803 data cover 2059 km^2 and streamer separation was 150 m, yielding a bin size of 37.5 × 12.5 m. The regional multiclient 2D seismic data (later reprocessed as CFI NBR) cover the entire Norwegian Barents Sea in four-line directions and with variable distances between each line (typically 3–5 km). The acquisition parameters were standardised using 8 km long 2D streamers through eight consecutive seasons from 2007 to 2014.

2.4. Seismic interpretation

Three regional seismic horizons were picked using regional 2D seismic data and used as input to generate Two-way-time (TWT) surfaces (base Paleocene, base lower Eocene and base middle Eocene) in Petrel software. Parts of these surfaces have been presented by Lasabuda et al. (2018a). Detailed horizon mapping was performed using the 3D seismic cubes SWB17 and NH-9803 tied to well 7216/11-1S to interpret five seismic horizons, H1–H5 (Fig. 4).

Three-dimensional seismic data reveal stratigraphic and geomorphological expressions that can be linked to sedimentary processes to understand the pattern of basin infilling (Posamentier and Kolla, 2003). We investigate the seismic interpretation using seismic facies analysis based on their appearance in map and line view (Fig. 5). Seismic amplitude reflection strength, internal geometry, and spatio-temporal pattern are inspected to determine each geomorphological feature including its depositional system and environment. We use the RMS

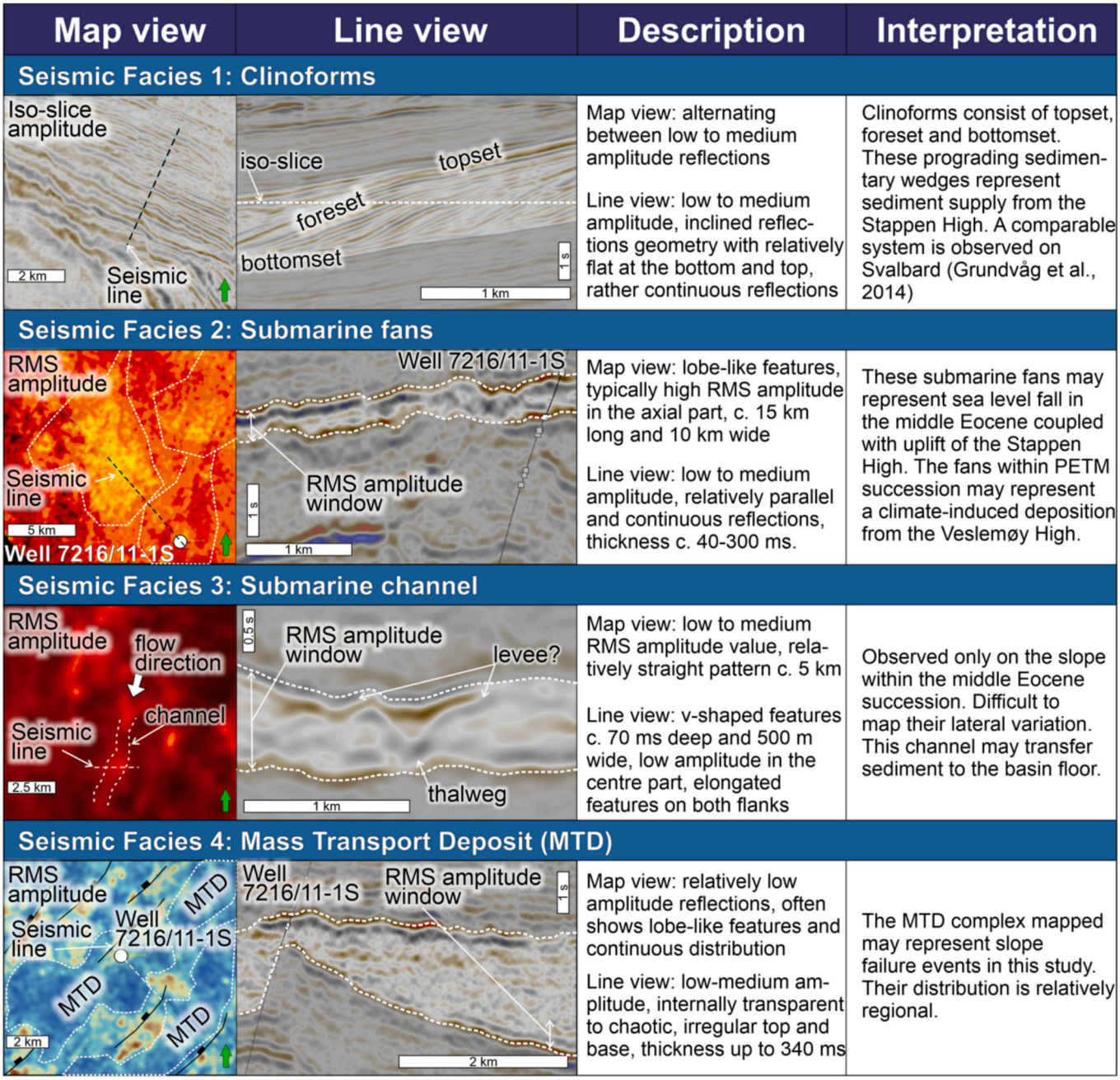

Fig. 5. Seismic facies analyses for the study area, highlighting their common appearances including the interpretation in map and line view.

amplitude seismic attribute to analyse the spatial distribution of seismic amplitude level (Sheriff, 1975; Taner and Sheriff, 1977). This method is commonly applied in scientific studies for both academic purposes and hydrocarbon exploration using 3D seismic data (e.g., Posamentier and Kolla, 2003; Lasabuda, 2013; Sømme et al., 2019).

The targeted PETM and EECO intervals have a P-wave velocity of approximately 2800 m/s with a frequency of around 20 Hz at the depth of the target, which gives a vertical resolution of c. 35 m (Safronova et al., 2014). In well 7216/11-1S, the PETM section is c. 40 m thick, which is above seismic resolution, allowing us to map out this succession using RMS amplitude seismic attribute extraction. However, in well 7316/5–1, the EECO is c. 20 m thick, which is below the seismic resolution. Therefore, we did not run an RMS amplitude seismic attribute analysis targeting this section.

2.5. *Stratigraphic forward modelling*

Numerical-based modelling was performed using the DionisosFlow software from BeicipFranlab to reproduce large-scale stratigraphic architecture and simulate basin filling. The deterministic approach of stratigraphic forward modelling (SFM) takes into account basin subsidence and uplift, eustatic sea level variations, sediment transport processes, wave actions, and climate conditions (Granjeon and Joseph, 1999; Hawie et al., 2017; Barabasch et al., 2019). The algorithm is built on an empirical diffusion model that is based on linear (hill-slope creeping) and non-linear (water discharge-driven transport) processes. In this empirical model, the sediment flux Q_s[km^2/year] is expressed as,

$$Q_s = \frac{-K_s}{\Delta h} - K_w Q_w^m S^n$$

Here, Δh [m] is the elevation change K_s and K_w [km^2/year] are the

diffusion coefficients for the slow creeping transport and the faster water-driven process, respectively, Q_w is the dimensionless local water discharge at the cell (characterised by 100 m^3/km^2), S is the local gradient of the basin slope, and m and n are dimensionless constants, usually chosen between 1 and 2 (Tucker and Slingerland, 1994).

We ran the simulations on the middle Eocene clinoform units because they are age-constrained and characterised by well data. Low, medium and high precipitation values were set to 130 and 140 (mm/year), 1300 and 1400 (mm/year), and 3900 and 4200 (mm/year). Sediment supply (Q_s) values were set to 20, 200 and 1000 (km^3/Ma). The other parameters were set as follows, diffusion coefficients (Ks = 3 and Kw = 5), sand content of up to 75 %, and fluvial discharge (Q_w) of up to 800 m^3/s. These values follow the modelling study of Lasabuda et al. (2024) and are considered a common practice, especially in addressing sandy deep-water systems (e.g., Hawie et al., 2018; Sangster et al., 2019).

3. Results

3.1. Stratigraphic descriptions from boreholes 7517/12-U-01 and 7418/1-U-1

3.1.1. 7517/12-U-01

Description: Borehole 7517/12-U-01 penetrates upper Paleocene strata near the Knølegga Fault immediately west of the Stappen High and shows a siltstone to fine-grained sandstone succession exhibiting a large-scale coarsening upwards trend (Figs. 1 and 3). Superimposed on this trend, the succession comprises a series of higher-frequency coarsening upward units, each around ten meters thick, which conform to classical shoreface-shelf parasequences (e.g., Colombera and Mountney, 2020).

Interpretation: We interpret these units to represent the successive basinward progradation of tide-dominated shoreface tongues (Fig. 3 and Supplementary Fig. 1). The strata occurring in the borehole thus represent the depositional environment prevailing in the Stappen High area prior to the PETM.

3.1.2. 7418/1-U-1

Description: Borehole 7418/01-U-01, located approximately 35 km south of the previous well, penetrates upper Paleocene to lower Eocene strata and shows a predominantly claystone to siltstone succession (Figs. 1 and 3). A prominent fine-grained sandstone interval and subordinate conglomerate layers occur within the otherwise fine-grained succession (Fig. 3).

Interpretation: Based on the overall relative grain size, structure, and degree of bioturbation, the fine-grained sandstone unit in the middle of the core is interpreted to be an inner shelf deposit, whereas the conglomerates represent storm-reworked outer shelf deposits (Supplementary Fig. 1). The finer-grained sections in borehole 7418/01-U-01 (e.g., depth shallower than 70 cm) are interpreted to record deposition in a low energy, outer shelf environment, below storm wave base (Fig. 3).

3.2. Correlation with other published boreholes and well data

We correlate from north to south, boreholes 7517/12-U-01 and 7418/1-U-1 (which have not been published earlier) with boreholes 7317/02-U-01, 7316/06-U-02, and 7317/10-U-01 (previously described by Sættem et al. (1994)) and publicly available exploration wells 7316/5–1 and 7216/11-S (Fig. 3). The three boreholes published by Sættem et al. (1994) show largely similar sedimentary style in terms of lithology, structures, and degree of bioturbation. According to available biostratigraphic data, borehole 7317/10-U-01 penetrates upper Paleocene strata while boreholes 7317/02-U-01 and 7316/06-U-02 penetrate middle Eocene strata and have been interpreted as storm-influenced inner shelf to outer shelf deposits (Fig. 3; Sættem et al., 1994).

Further south, Paleocene–Eocene strata are penetrated by exploration wells 7316/5–1 and 7216/11-1S (Figs. 3 and 4). The Paleocene–Eocene succession occurring in the Sørvestsnaget Basin (7216/11-1S) is dominated by greyish mudrocks (Supplementary Fig. 2). Based on drill cuttings, these fine-grained deposits are interpreted to be deposited in a low energy deep marine setting, although the accompanying gamma-ray logs occasionally show low values, which may indicate the presence of volcanic tuffs (Supplementary Fig. 2; Ryseth et al., 2003). Following biostratigraphic analysis, the volcanic rocks (sills) occurring in well 7316/5–1 are related to the early Eocene plate breakup and may thus be correlated with the PETM (Fig. 3). These sills are typically recorded as high-amplitude reflections in the seismic data (Supplementary Fig. 3; Fig. 4).

Thick middle Eocene strata occur in both wells 7316/5–1 and 7216/11-1S and are dominated by mudrocks interpreted to be deep-marine deposits. In addition, clean, greyish, fine-grained sandstones with a blocky to erratic gamma-ray signal occur in both wells, which from previous core descriptions, are interpreted as turbidite sandstones (Ryseth et al., 2003). As such, the north-south borehole-well transect appears to record a middle Eocene deepening trend from a shoreface/inner shelf setting to a relatively deep marine setting (Fig. 3).

Apectodinium Augustum dinoflagellates, which is typically associated with the PETM event elsewhere (e.g., Sluijs and Brinkhuis, 2009; McNeil and Parsons, 2013; Berndt et al., 2023; Sømme et al., 2023), are documented in a 110 m thick interval (levels 3410–3300 m) in well 7316/5–1 and in a 40 m thick interval (levels 3410–3370 m) in well 7216/11-1S (Fig. 3; Equinor, 2023). *Azolla Acme* (freshwater ferns), which are considered an ecological response to the EECO event (e.g., Brinkhuis et al., 2006; Barke et al., 2012) are present in a 14 m thick interval (levels 3114–3100 m) in well 7316/5–1 and in a 20 m thick interval (levels 3190–3170 m) in well 7216/11-1S (Fig. 3; Equinor, 2023).

There are no available biostratigraphic data for borehole 7418/1-U-1, making a correlation to the PETM and EECO events a speculative attempt. They are most likely eroded due to post-depositional reworking processes, for example by wave/storm activity (Fig. 3). If they are present at this location but have not been sampled due to a larger sampling interval, then we suspect the corresponding sedimentary layers representing the hyperthermal events to be very thin.

3.3. Seismic facies and seismic geomorphology

3.3.1. Seismic facies 1: Clinoforms

Description: SF1 shows low to medium amplitude, inclined reflections geometry with relatively flat at the bottom and top, and continuous to semi-continuous reflections. This seismic facies shows SW-directed sigmoidal prograding features extending basinward (down-dip) for c. 40 km and traceable along strike for distances up to 50 km (Fig. 5).

Interpretation: SF1 is interpreted as a clinoform (sensu Steel and Olsen, 2002), which consists of a topset, foreset and bottomset. These prograding sedimentary wedges represent sediment supply from the north. A comparable clinoform system with a similar age (middle Eocene) is observed on Svalbard (e.g., Helland-Hansen and Grundvåg, 2021).

3.3.2. Seismic facies 2: Submarine fans

Description: SF2 shows low to high amplitude, relatively parallel and continuous reflections, and a thickness of about 40 ms. On the map view, this seismic facies shows lobe-like features with a dimension of c. 15 km long and 10 km wide and typically exhibits high RMS amplitude in the axial part (Fig. 5). Stacking together, these lobe-like features can reach a thickness of 300 ms with a dimension of c. 150 km long and 40 km wide.

Interpretation: SF2 indicates depositions of submarine fans. These fans are a product of gravity-driven current, which travelled along the slope and was deposited on the basin floor. Core descriptions at the submarine fans interval from well 7216/11-1S suggest sandy successions (Fig. 3; Ryseth et al., 2003).

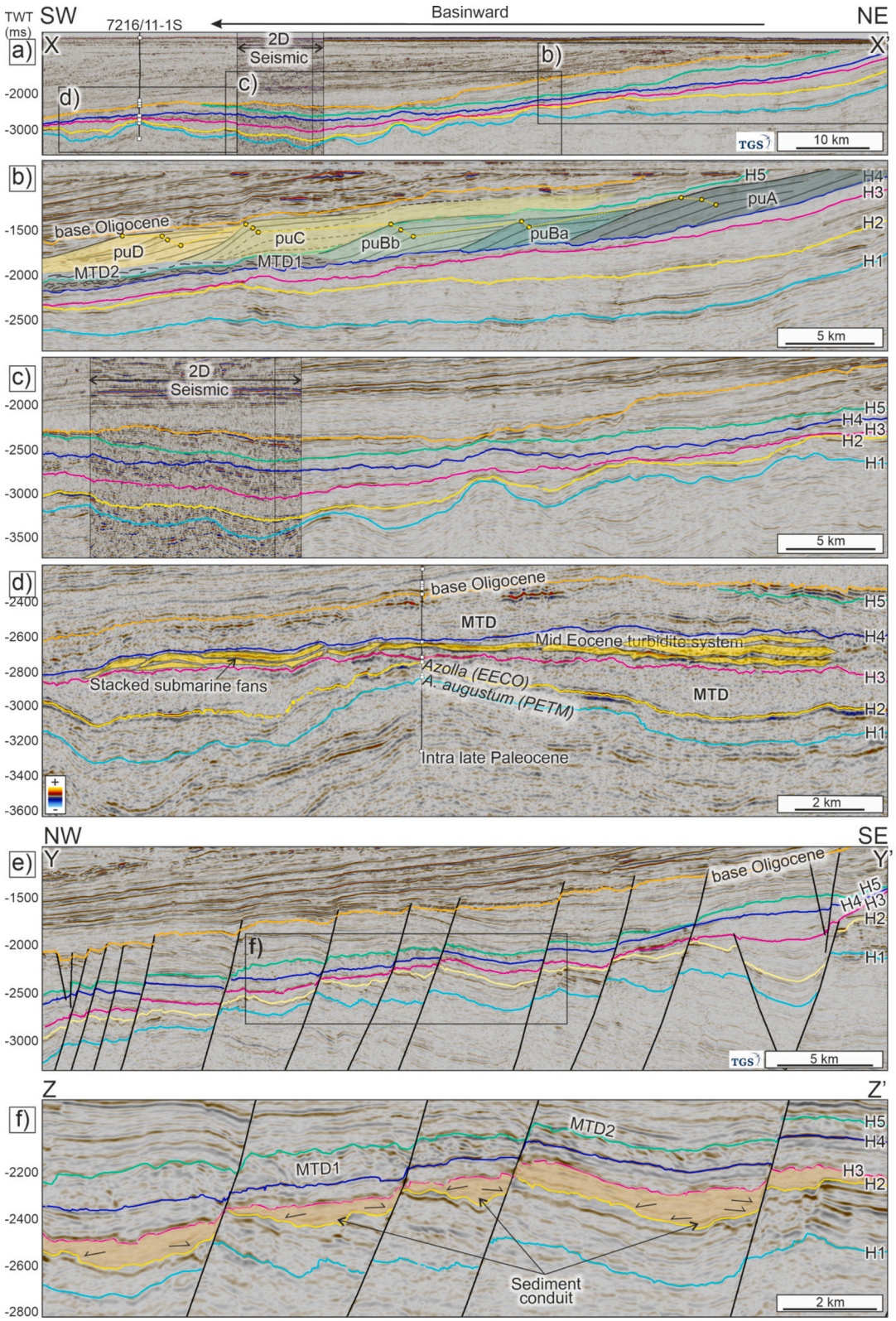

Fig. 6. Seismic stratigraphy from shelf to basin floor. a) NE-SW-oriented seismic profile shows regional seismic stratigraphy tied to well 7216/11-1S. See rectangles for zoom-in seismic profiles b, c and d. b) A set of shelfal clinoforms (making up clinothems puA – puD) are shown, including their trajectory analyses. Mass-transport deposits (MTDs 1 and 2) are observed on seismic horizons H4 and H5. c) slope profile in the study area shows undulated morphology, suggesting complex compressional events (e.g., see seismic horizon H1). d) basin-floor area with well-tops from well 7216/11-1S. See the middle Eocene turbidite system between seismic horizon H3 and H4 as described in (Ryseth et al., 2003) and (Safronova et al., 2012, 2014). A correlation of *A. Augustum* indicating the PETM with the seismic data and the occurrence of the *Azolla Acme* indicating the EECO are shown in the well location. e) NW-SE-oriented seismic profile showing rotated fault blocks. See the rectangle for zoom-in seismic profile f. f) A middle Eocene sediment conduit system is located above seismic horizon H2, and MTD1 and MTD2 are shown. Vertical exaggeration is 5×. For uninterpreted seismic profiles, see Supplementary Fig. 4. For the location of the seismic profiles, see Fig. 1a.

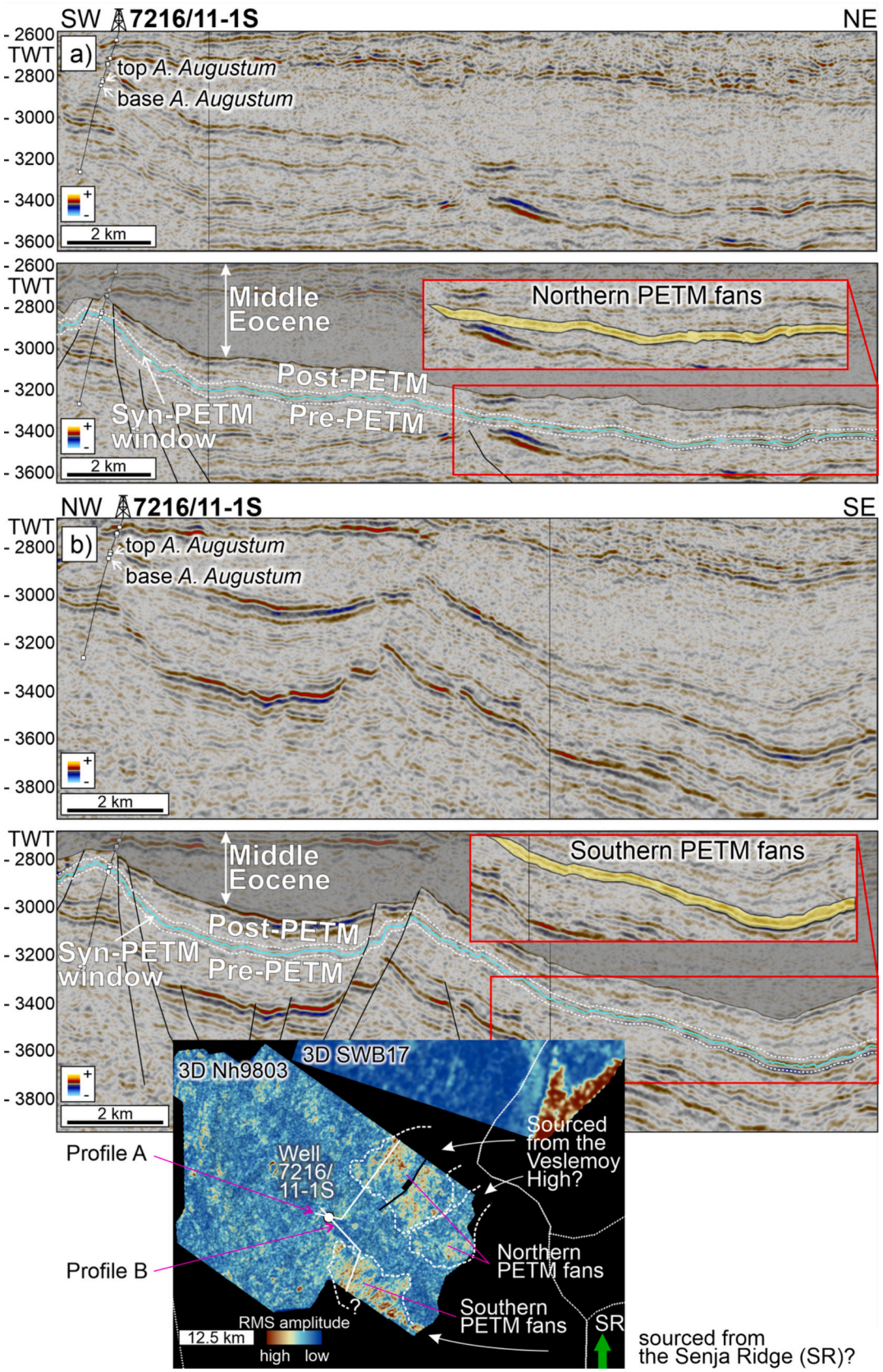

Fig. 7. PETM submarine fans. a) Northern PETM fans, b) Southern PETM fans. Inset: the lateral extent of both PETM fans with their interpreted sediment routing.

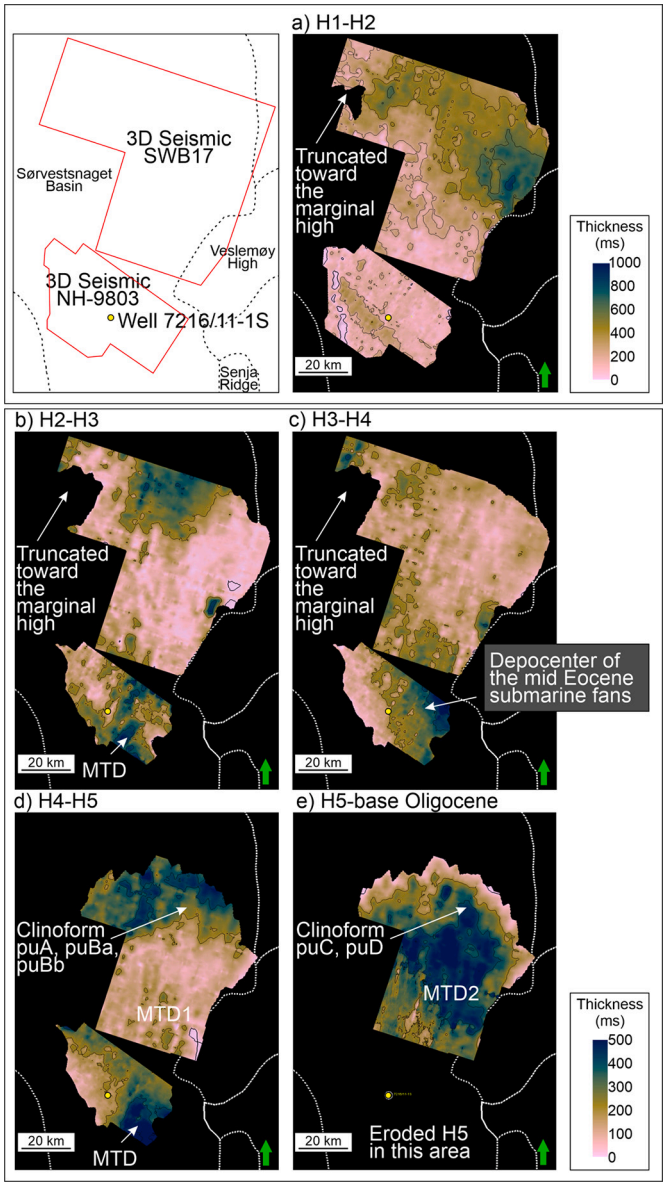

Fig. 8. Time thickness maps (ms). a) H1-H2, b) H2-H3, c) H3-H4, d) H4-H5, e) H5-base Oligocene.

3.3.3. Seismic facies 3: Submarine channel

Description: SF3 shows low to medium-amplitude reflections and u- and v-shaped features of about 70 ms deep and c. 500 m wide. In the axial part, it shows low amplitude with elongated features on both flanks. On the map view, this seismic facies displays a relatively straight pattern of about 5 km (Fig. 5).

Interpretation: SF3 is interpreted as the development of a submarine channel. This channel is only observed on the slope within the middle Eocene succession. The channel might transfer sediment to the basin floor and evolve into submarine fans. However, it was difficult to map its lateral variation.

3.3.4. Seismic facies 4: Mass Transport Deposit (MTD)

Description: SF4 shows low to medium amplitude, transparent to chaotic internal reflections and irregular top and base with a thickness of up to 340 ms. On map view, this seismic facies shows lobe-like features and a relatively continuous distribution (Fig. 5).

Interpretation: SF4 suggests a deposition of mass transport deposit (MTD). The MTDs may represent slope failure events and were deposited following gravity-driven processes.

3.4. Seismic stratigraphy

3.4.1. Seismic horizon H1

Seismic horizon H1 corresponds to the base of the Eocene succession. It overlies a series of folds on the slope and basin floor (Fig. 6a, c). The first and last occurrence of *A. Augustum,* indicating the PETM window is found at c. 20 m above and below seismic horizon H1 in well 7216/11-1S, giving a total thickness of c. 40 m *syn*-PETM succession. Within the syn-PETM, we observe an appearance of seismic facies SF2 (submarine fans). Two key clusters of SF2 are observed from the RMS amplitude map; the northern and southern PETM fans (Fig. 7a, b). They are about 40 ms thick and relatively thinner than the middle Eocene fans (see below). The northern PETM fans are oriented in the NE-SW direction, while the southern PETM fans are in the NW-SE direction (Fig. 7a, b). The interval between seismic horizons H1 and H2 shows a maximum thickness of about 1000 ms, located in northeast of the study area (Fig. 8a).

3.4.2. Seismic horizon H2

Seismic horizon H2 corresponds to the base of middle Eocene succession and is relatively continuous throughout the study area (Fig. 5a, b). The *Azolla Acme*, indicating the EECO is found 13 m above the seismic horizon H2 in well 7216/11-1S (Fig. 4) However, the EECO succession (20 m) is thin and below the seismic resolution used in this study (35 m) and therefore, it cannot be mapped (see above). Between seismic horizons H2 and H3, we observe a relatively low amplitude seismic unit extending from the shelf to the deep sea, often represented by seismic facies SF4 – mass transport deposits (MTD) (Fig. 6a-d). On the slope, the structural development shows rotated fault blocks, indicating rifting processes. Seismic onlapping patterns towards the seismic horizon H2 suggest sediment conduit, transferring sediments from the slope to the basin floor (Fig. 6f). Isopach thickness map of the unit between seismic horizons H2 and H3 shows a thick interval in the north of 3D Seismic SWB17 and in the deep basin (3D Seismic NH-9803) (Fig. 8b).

3.4.3. Seismic horizon H3

Seismic horizon H3 corresponds to the base of the middle Eocene turbidite system. On the shelf, the unit above seismic horizon H3 shows predominantly low amplitude reflections (Fig. 6). On the slope, seismic profiles and the RMS amplitude map 50 ms above seismic horizon H3 show seismic facies SF3, suggesting sediment transfer through submarine channels (Figs. 6, 7d). On the basin floor, the seismic horizon H3 exhibits seismic facies SF2 (submarine fans). The geomorphology of these submarine fans has previously been described as a stacked series of individual fans that altogether covered an area of 40–100 km wide and up to 150 km long by Safronova et al. (2014) using 3D seismic data (NH9803 3D cube which is also included in this study, see Fig. 1a). Main depocenter of the unit between seismic horizons H3 and H4 is located in the east of well 7216/11-1S (Fig. 8c)

3.4.4. Seismic horizon H4

Seismic horizon H4 corresponds to the top of the middle Eocene turbidite system in well 7216/11-1S. This seismic horizon shows an irregular surface throughout the study area (Fig. 6b). On the shelf, the unit above seismic horizon H4 shows seismic facies SF1 (Clinoforms) (Fig. 6b). The mapped clinoroms are here called puA, puBa and puBb, following Safronova et al. (2014). On the slope, seismic facies SF4 (MTD) is observed above the seismic horizon H4, which is named MTD1 (Figs. 6f, 8d).

Following the nomenclature proposed by Helland-Hansen et al. (2012), we interpret the mapped clinoforms to be shelf prism-type rather than shallow marine/delta-type clinoforms based on their dimensions (100's m thick) and their relative positions on the reconstructed paleoenvironments according to borehole data (Figs. 1a and 3).

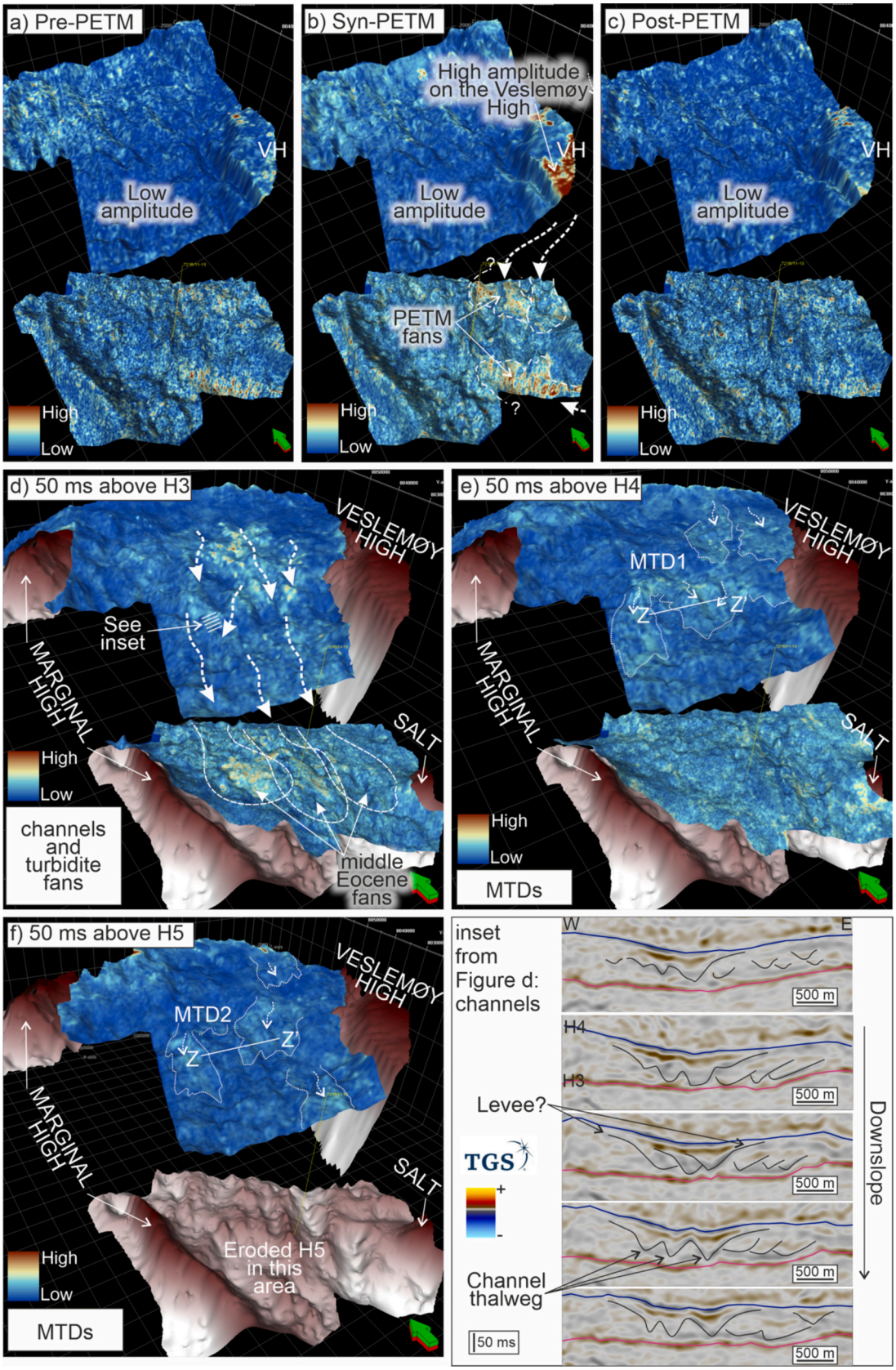

(caption on next page)

Fig. 9. 3D view of Root Mean Square (RMS) amplitude seismic attribute maps and their geomorphological interpretations. a) Pre-PETM using RMS amplitude extraction window of 10 ms below *syn*-PETM succession. b) Syn-PETM using RMS amplitude extraction window of 20 ms, consisting of 10 ms below and above seismic horizon H2. PETM fans are shown. c) Post-PETM using RMS amplitude extraction window of 10 ms above syn-PETM succession. d) RMS amplitude map extracted from 50 ms above seismic horizon H3 shows slope channels and turbidite fans on the basin floor. e) RMS amplitude map extracted from 50 ms above seismic horizon H4 shows extensive mass transport deposits (MTDs), named MTD1. f) RMS amplitude map extracted window of 50 ms above seismic horizon H5 shows MTD2 on the slope. Note that seismic horizon H5 is truncated under base Oligocene surface in the basin-floor area (Fig. 6d). Inset seismic profiles from (d) show an evolution of channel systems downslope. Each seismic profile is separated by c. 240 m. Channel thalweg developments include likely levee systems on both flanks. Vertical exaggeration is 10×. For uninterpreted maps and seismic profiles, see Supplementary Fig. 5. For orientation of the location of maps, see Fig. 1a. The location of Z-Z' for profile in Fig. 6 is shown.

These shelf-edge clinoforms appear to be gently dipping (1–3°) with high relief (c. 200 m), even without decompaction analysis. Isopach thickness map shows a combined thickness of up to 500 ms on the proximal area, containing the clinoforms puA, puBa and pub (Fig. 8d).

3.4.5. Seismic Horizon H5

Between seismic horizon H5 and the base Oligocene horizon, other packages of seismic facies SF1 are observed, which are called puC and puD (Safronova et al., 2014). The topset part of these clinoforms is not very well preserved due to erosion and deposition of glacial sediments of the Bjørnørennna trough mouth fans (Fig. 5a). On the bottomset of these prograding units, another chaotic reflection package typical seismic facies SF4 (MTD) is found and, here named MTD2 (Fig. 6f). The seismic horizon H5 is truncated under the base of Oligocene in the basin floor area (Figs. 6e and 8e). Isopach thickness map shows a southward-shifted deposition, containing clinoforms puC and puD (Fig. 8e).

4. Discussion

4.1. The pattern of basin filling in Sørvestsnaget Basin

A combination of boreholes, wells and seismic data makes it possible to interpret changing paleoenvironments and source-to-sink sediment pathways in the Sørvestsnaget Basin onwards from the Paleocene–Eocene transition (c. 56–55 Ma) to the late Eocene (c. 34 Ma). According to our analysis, we recognise four stages of development (Fig. 10).

4.1.1. Stage 1a (Pre-PETM)

Pre-PETM (late Paleocene) is characterised by pelagic-hemipelagic deposition based on well data (Fig. 3; Ryseth et al., 2003), suggesting that the central part of the Sørvestsnaget Basin formed predominantly deep marine conditions (Lasabuda et al., 2018a). These deep marine conditions were being shallower (from outer shelf to shoreface) towards the Stappen High, evidenced by paleoenvironmental reconstructions using shallow boreholes (Fig. 3; Sættem et al., 1994). Therefore, the main sediment input is inferred from the Stappen High as the other structural highs (i.e. Veslemøy High and Senja Ridge) were part of a vast basin development during the Paleocene (Eidvin et al., 1993; Faleide et al., 1993).

4.1.2. Stage 1b (Syn-PETM)

Syn-PETM event (c. 55.9 Ma) largely coincides with the major plate break-up (c. 55 Ma) to the west of the study area (Faleide et al., 2008). During the PETM, sediments likely entered the Sørvestsnaget Basin from the north and northeast (Fig. 10). The overall deep marine setting occurred in the wider SW Barents Sea area as suggested by a paleobathymetrical reconstruction (Lasabuda et al., 2023). Sedimentation in the basin was probably dominated by hemipelagic suspension settling and likely modest sediment input from the catchment areas (the Stappen High and parts of Senja Ridge), based on regional mapping and an increase in sedimentation rate at the onset of the Eocene in the Sørvestsnaget Basin as reported by Lasabuda et al. (2018a) (Fig. 4a).

The first episode of the Cenozoic exhumation in the southern part of Stappen High, Veslemøy High and Senja Ridge was later in the middle Eocene (postdate the PETM fans) based on apetite fission track analysis (Green and Duddy, 2010). Therefore, the northern and southern PETM fans indicate a climate-influenced deposition from paleo-highs. However, it is not clear where the source area is for the PETM fans. Although the Veslemøy High were likely part of an epeirogenic basin during the early Eocene (Ryseth et al., 2003), some parts remain above sea level at around the PETM time based on numerical modelling (Lasabuda et al., 2023). This suggests Veslemøy High as a potential source area for the northern PETM fans (Fig. 7a). On the Senja Ridge, the earliest Eocene succession is truncated below the younger glacial strata (Eidvin et al., 1993), indicating that nominating this ridge as the source for the southern PETM fans remains a speculation (Fig. 7b). Recent multi-source-to-sink modelling for the early Eocene suggests that a paleo-high was likely formed along the northeastern area extended from the Stappen High (Lasabuda et al., 2024), which may suggest another candidate for the sediment source for these PETM fans, posing a longer sediment transport route to the fans.

Due to the lack of biostratigraphic data from the studied borehole, the PETM is not very well expressed in the Stappen High area, although it is well documented in the drill cores further north in the Central Tertiary Basin, Spitsbergen (Dypvik et al., 2011). In the Vestbakken Volcanic Province, the interval of the PETM is represented by the occurrence of volcanic rocks (Fig. 8). This volcanism has largely been attributed to the North Atlantic Igneous Provinces (NAIP) contributing to a major release of methane leading to the temperature increase during the PETM (Svensen et al., 2004; Hovikoski et al., 2021; Jones et al., 2023).

4.1.3. Stage 1c (post-PETM)

The sedimentation pattern is comparable to the pre-PETM conditions, according to well data and RMS amplitude seismic attribute analysis (Figs. 4 and 9). During post-PETM, sediment deposition was likely through pelagic/hemipelagic in a deep marine setting, with no observable deposition of submarine fans (Fig. 10).

The early Eocene was generally characterised by high precipitation and fresh-water runoff rates (Greenwood et al., 2010), eventually contributing to and possibly triggering the Azolla bloom (c. 49 Ma) that has been recorded further north on the Lomonosov Ridge in the Arctic Ocean (Brinkhuis et al., 2006) and to the south in the North Sea (Barke et al., 2012). However, due to the lack of biostratigraphic data from the shallow cores, the EECO is not clearly documented in the shallow borehole locations and is thin (below seismic resolution) at the studied well locations, which prevents us from lateral mapping using present seismic data (see above).

4.1.4. Stage 2 (earlier middle Eocene, c. 45 Ma)

For the middle Eocene, our combined cores, wells and seismic data indicate paleoenvironments ranging from shoreface to deep marine (Figs. 3 and 6). On the slope, sediments were transferred through sediment conduits, whose positions and development seem to be controlled by the rotated fault block development (Fig. 6e, f). The transtensional nature of the basin in the middle Eocene is responsible for the tilting of the fault blocks during a *syn*-tectonic phase (Fig. 6f; Kristensen et al., 2018). These sediment conduits are overlain by submarine channels (Fig. 6f). It is possible that these conduits have evolved to become submarine channels through turbiditic current reorganisation (e.g., Pirmez and Imran, 2003; Mitchell et al., 2021). These channels likely

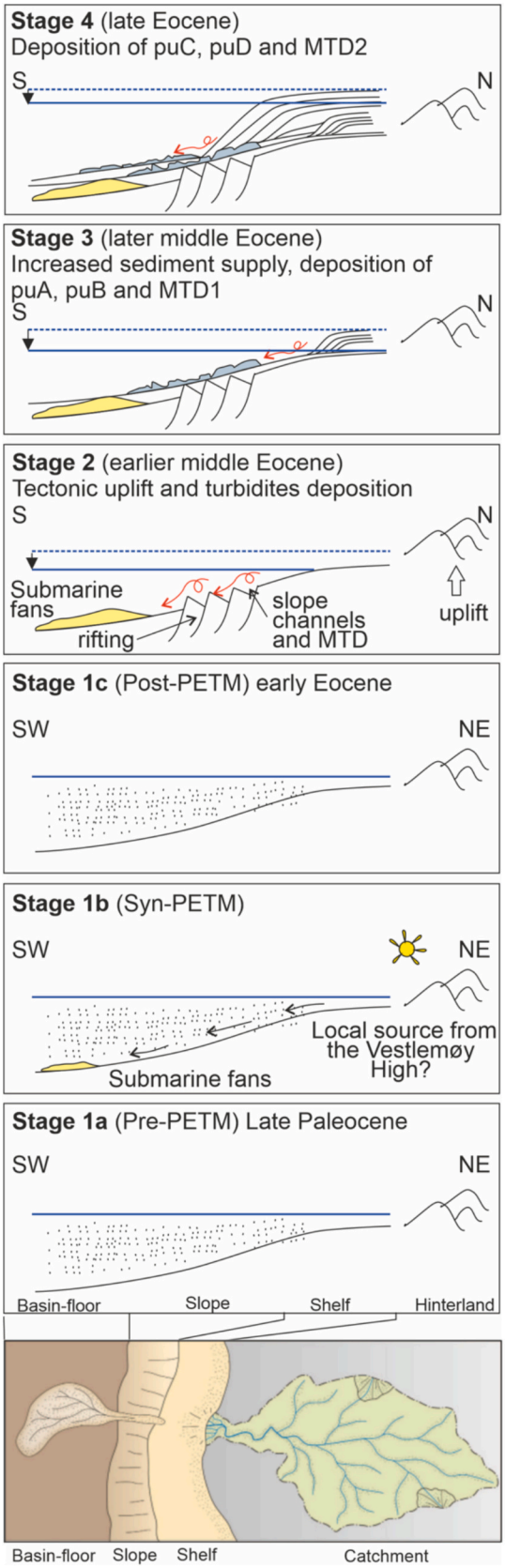

Fig. 10. Conceptual model of the depositional systems in response to Paleocene-Eocene tectonic and climatic forcings (Stage 1–4). Note the sediment transfer is described from the hinterland to the basin-floor area, including its relative sea level. The plan view figure at the bottom is modified from Helland-Hansen et al. (2016). See the main text for a detailed discussion of the various stages.

transported sediments into the basin to form sandy turbidite fans, following southward sediment routing pattern suggested by Flowerdew et al. (2023) using provenance analaysis (Fig. 9d).

These submarine fans are referred to as du1 by Safronova et al. (2014). Based on new 3D seismic data, we proposed that these fans were deposited before the deposition of clinothems puA-puD. Major eustatic sea-level fall in the middle Eocene (Miller et al., 2005, 2020) could be a triggering mechanism for this event (Fig. 4). These sandy fans at the Sørvestsnaget Basin could also be related to the contemporaneous uplift of the Stappen High and the northern Barents Sea due to the Eurekan deformation event which eventually caused compression/transpression between the Greenland and Svalbard/Barents Shelf margin (Bergh et al., 1997; Faleide et al., 2015; Doré et al., 2016; Lasabuda et al., 2021).

Rising relative humidity in the Arctic during the middle Eocene, c. 45 Ma (Jahren and Sternberg, 2003, 2008) could have amplified the transfer of sand coupled with increased weathering and riverine runoff in the catchment area. This climatic factor has also been attributed to the deposition of middle Eocene sand in a nearby basin on Svalbard (Grundvåg et al., 2023).

4.1.5. *Stage 3 (later middle Eocene, c. 43 Ma)*

A significant increase in sediment supply to the basin is suggested by the progradation of clinoforms puA and puB (Fig. 6a, b). This high sediment input was likely a result of a larger catchment and longer runoff from the uplifted Stappen High as the main source area (Fig. 11; Lasabuda et al., 2021). Both clinoforms puA and puB (puBa and pub) show ascending shelf-edge trajectories, indicating increasing sediment supply during relative sea-level rise (Fig. 6a, b). Clinoform puBa onlaps towards the clinoform puA, suggesting a forced regression during an episode of sea-level fall (Figs. 4a, 6b). The downlapping reflection pattern of puBb on top of MTD1 shows that MTD1 predates the puBb (Fig. 6b). The MTD1 may be emplaced during a period of sea-level fall before the shelf progradation of puBb commenced (Fig. 6b). The deposition of MTD here can be caused by fault movements/seismic activity of the underlying fault system. However, considering high sedimentation rates during these times, we suggest that they were likely triggered by high sediment input causing oversteepening and shelf-edge/slope collapse.

4.1.6. *Stage 4 (late Eocene, c. 37 Ma)*

The last sets of clinoforms (puC and puD) were deposited during this stage (Fig. 6b). Relative sea-level fall at the transition from puBb to puC may have initiated the deposition of MTD2 (Fig. 4a). Parts of puC and puD prograded over the MTD2 indicating that MTD2 predates the deposition of puC and puD (Fig. 6b). Rising trajectory for both puC and puD suggests relatively high rates of sediment supply, which kept up with the rates of relative the sea level rise (Fig. 6b).

The MTD1 and MTD2 in stages 3 and 4 are equivalent to du2 and du3 of Safronova et al. (2014). Based on new 3D seismic data, we extend their interpretation on the slope area where these features represent mass transport deposits based on seismic facies SF4 as a typical expression of MTD and observed on RMS amplitude maps (Figs. 5, 6e, f and 9e, f). The MTD1 and MTD2 later evolved to form submarine fans on the basin floor as a result of downslope-travelled turbiditic current (Safronova et al., 2014).

4.2. *Role of climate and tectonics on sediment transfer in the SW Barents Sea and implications to Arctic source-to-sink*

We performed a sensitivity analysis using stratigraphic forward modelling (SFM) to test the influence of tectonic and climatic perturbation on sediment transfer in the SW Barents Sea. Here tectonic force is

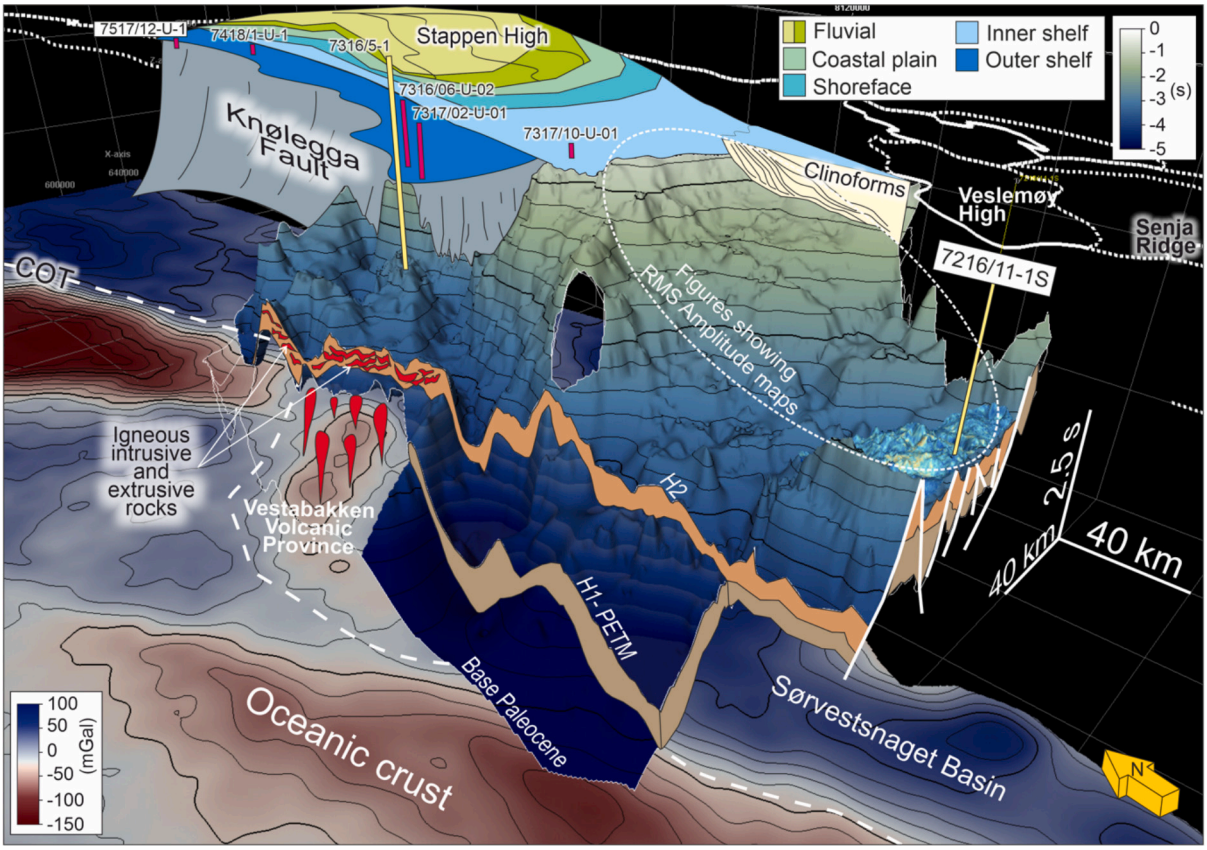

Fig. 11. Axonometric view of the general Eocene paleoenvironment in the SW Barents Sea. Paleoenvironment during early Paleocene (volcanism) and Eocene (inferred fluvial to deep marine). Two-way time (TWT) seismic surfaces of the base of Paleocene (seismic horizon H1 - PETM) and the base of middle Eocene (seismic horizon H2) are adapted from Lasabuda et al. (2018a). The underlying free-air gravity map shows the continental and ocean transition represented by a long-dashed line (Dumais et al., 2022). The oceanic crust is characterised by negative anomaly shown as reddish colour. Vertical exaggeration of 10×. For an uninterpreted seismic profile showing the volcanic complex, see Supplementary Fig. 3.

represented by a major increase in sediment supply or Qs (km^3/ Ma) and climate dynamics are represented by precipitation and evaporation (mm/year).

The impact of tectonics (e.g., uplift of the source areas) on delivering sand to the basin can be seen from a significant increase in sand content (e.g., Fig. 12a, b, c). We also observe major thickening when sediment supply is increased (e.g., Fig. 12a, d, g). However, climatic conditions (i.e., precipitation and evaporation) appear to control sand transport variability to the basin (e.g. Fig. 12b, e, h). By increasing precipitation and evaporation, the temporal evolutionary pattern of the sand is much more variable (e.g., Fig. 12a, g).

This model may explain the preconditioning nature of PETM that can generate depositions of submarine fans found in this study in the Norwegian Arctic due to higher temperature and weathering, increased fluvial runoff, and frequent river floods leading to higher erodibility of sediments (e.g., Dypvik et al., 2011; Foreman et al., 2012; Grundvåg et al., 2023). A hyperthermal may have changed the dynamics of the source-to-sink systems, which has also been reported in the North Sea and the Norwegian Sea (Sømme et al., 2019, 2023). A recent global compilation shows that hyperthermal events contribute to deep-sea sand deposition, regardless of their latitudinal position (Burton et al., 2023).

Lateral tectonic plate separation that creates a deep-water connection between oceans can also influence the type of sediment transport in a basin through, for example, ocean bottom currents (e.g., Hernández-Molina et al., 2008; Rebesco et al., 2014). Based on our seismic mapping, we did not observe features indicating contourites or sediment drift (Figs. 5 and 6). This is probably because in the study area, the Fram Strait, the only nearby deep-water gateway connecting the Arctic and Atlantic oceans was opened later in the Miocene, c. 17 Ma (Jakobsson et al., 2007; Engen et al., 2008). Moreover, the Barents Seaway remains closed during much of the Cenozoic (Lasabuda et al., 2023) and opened up later in the Quaternary, at c. 690.000 ka (Patton et al., 2024).

The majority of the clinoform systems in the circum-Arctic are strongly linked to relatively coeval tectonic events. Our middle Eocene clinoforms (puA and puB) and those mapped in Spitsbergen show that the Eurekan compression that resulted in uplifted source areas strongly influenced sandy sediment transfer to the basin floor (Helland-Hansen and Grundvåg, 2021; Lasabuda et al., 2021; Grundvåg et al., 2023). This tectonic force may be linked to synchronous exhumation events in the circum Arctic based on apatite fission tracks analysis (Green and Duddy, 2010; Japsen et al., 2023). Our late Eocene clinoform systems (puC and puD) are synchronous with clinoform systems in the Chukchi region (Hegewald and Jokat, 2013) and in the NE Greenland (Petersen, 2021), which are correlated to a late Eocene uplift event identified by Japsen et al. (2014). However, Hovikoski et al. (2021) suggest that the clinoforms in the basins on the Northeast Greenland Shelf were formed earlier in the middle Eocene. This discrepancy shows that the sparsity and lack of accurate geochronology due to limited data is a major challenge when working in a remote and underexplored region such as the Arctic.

5. Conclusions

We have investigated sedimentary stacking patterns and basin-fill development in the Sørvestsnaget Basin, on the Barents Shelf, Norwegian Arctic using a combination of new 3D seismic data, shallow cores and exploration wells, and linked them to Paleocene–Eocene tectonic and climatic forcing. Below are key highlights from our findings:

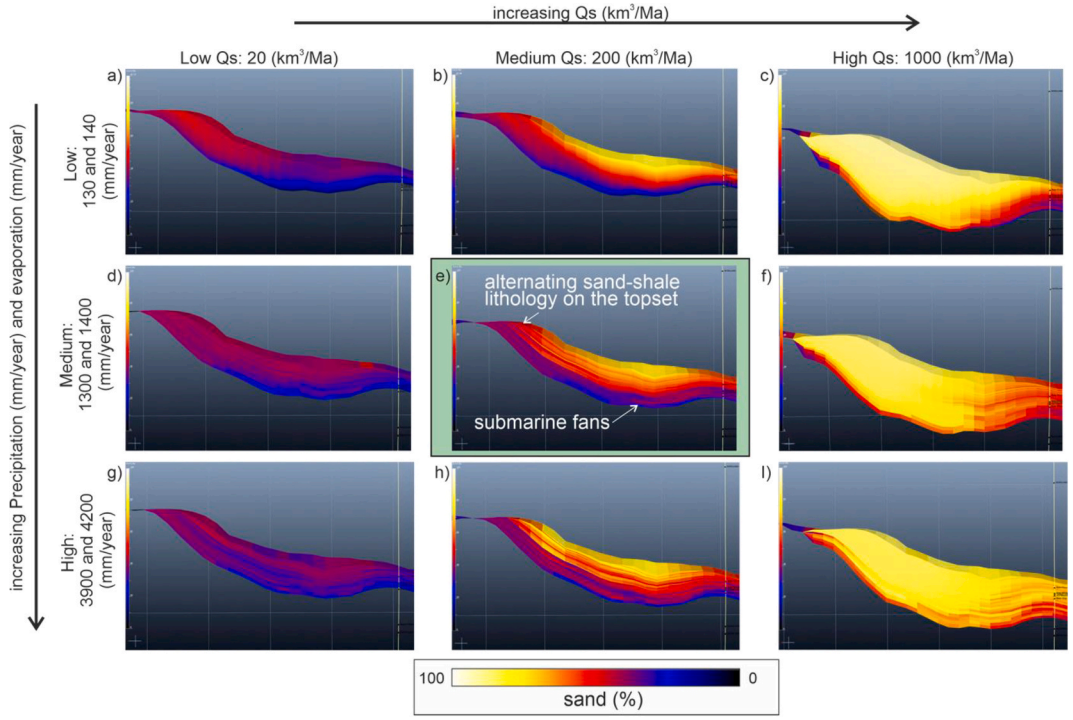

Fig. 12. Stratigraphic Forward Model (SFM) of testing influence of tectonic manifestation represented by a major increase in sediment supply or Qs (km^3/ Ma) and climate perturbation represented by precipitation and evaporation (mm/year), following parameters used by Lasabuda et al. (2024). a) Low Qs and low precipitation and evaporation; b) medium Qs and low precipitation and evaporation; c) High Qs and low precipitation and evaporation; d) Low Qs and medium precipitation and evaporation; e) Medium Qs and medium precipitation and evaporation show the best-fit model (green rectangle); f) high Qs and medium precipitation and evaporation; g) Low Qs and high precipitation and evaporation; h) medium Qs and high precipitation and evaporation; i) high Qs and high precipitation and evaporation. Yellow represents sand, dark blue represents shale.

- The Paleocene-Eocene Thermal Maximum (PETM) succession defined by the occurrence of *Apectodinium Augustum* in well 7216/11-1S was traced across the Sørvestsnaget Basin using 3D seismic data. Our mapping indicates, for the first time, depositions of the PETM submarine fans that were deposited under a hyperthermal condition without any obvious link to a tectonic uplift episode. These climate-influenced fans show an individual fan, likely as a result of a single depositional event compared to the middle Eocene tectonic-driven fans earlier mapped by Safronova et al. (2014) that display stacked submarine fans, probably deposited during multi-phase or episodic events. The Early Eocene Climate Optimum (EECO) succession constrained by the occurrence of *Azolla Acme* in well 7216/11-1S is, however, too thin (c. 20 m) to be mappable under the present 3D seismic resolution (c. 35 m).
- Our study revisited the work of Safronova et al. (2014) in the light of new 3D seismic data that cover predominantly the shelf-slope area, suggesting 1) the development of a slope channel system that transported sediment to the basin floor, 2) the emplacement of mass transport deposits (MTD) called MTD1 and MTD2, which then evolved to become submarine fans, and 3) that the deposition of middle Eocene turbidite fans predates the deposition of clinoform puA, which shows an ascending shelf-edge trajectory.
- The depositions of submarine fans, MTDs and shelf-edge clinoforms in the middle-late Eocene were likely associated with tectonic uplift of the Stappen High coupled with a series of global eustatic sea-level falls. This system can be correlated across the circum-Arctic with other comparable sediment prograding wedges, pointing to a synchronous exhumation pattern in the Eocene linked with plate movement and magmatism.
- Our forward stratigraphic modelling shows that tectonic uplift significantly increased the amount of sand delivered to the basin as documented by a thickening of the basin fill succession, while climatic factors influence the variability of sand transport and depositional patterns. This numerical modelling result may explain the differential dimension thickness and character between the tectonically induced submarine fans with the climate-driven ones.

Author contributions

A.P.E.L. led the interpretation of the seismic data and well-logs, performed the forward stratigraphic modelling, wrote the original manuscript, and drafted the figs. A.H. initialised a bigger scope of the modelling study. I.E. contributed to the detailed core description and interpretation with input from S.-M. K who also provided access to the core laboratory. The shallow core investigations were part of the I.E.'s master thesis. B.K. was involved in the acquisition and processing of the seismic data. T.S. provided input to biostratigraphic analysis. All authors contributed to the synthesis and integration of the observational datasets and reviewed the manuscript.

CRediT authorship contribution statement

Amando P.E. Lasabuda: Writing – original draft, Visualization, Validation, Software, Methodology, Investigation, Formal analysis, Conceptualization. **Domenico Chiarella:** Writing – review & editing, Validation, Supervision, Software, Project administration, Investigation, Formal analysis, Conceptualization. **Tor Oftedal Sømme:** Writing – review & editing, Validation, Resources, Investigation, Formal analysis, Conceptualization. **Sten-Andreas Grundvåg:** Writing – review & editing, Validation, Investigation, Formal analysis. **Isak Eikelmann:** Writing – review & editing, Investigation, Formal analysis, Data curation. **Stig-Morten Knutsen:** Writing – review & editing, Validation, Supervision, Project administration, Investigation, Data curation, Conceptualization. **Anthony George Doré:** Writing – review & editing,

Validation, Investigation. **Jan Sverre Laberg:** Writing – review & editing, Supervision, Project administration, Investigation, Funding acquisition, Conceptualization. **Tom Arne Rydningen:** Writing – review & editing, Validation, Investigation. **Alfred Hanssen:** Writing – review & editing, Supervision, Project administration, Funding acquisition, Conceptualization. **Bent Kjølhamar:** Writing – review & editing, Visualization, Software, Investigation, Data curation.

Declaration of competing interest

There are no conflicts of interest.

Data availability

Seismic data were provided with courtesy of TGS and are not publicly available. Any requirement for accessing seismic data can be addressed directly to TGS (https://www.tgs.com/contact-us). Well-logs and well-tops are publicly available through the DISKOS database (https://www.sodir.no/en/diskos/) of the Norwegian Offshore Directorate (NOD), previously called the Norwegian Petroleum Directorate (NPD). Core data can be accessed through the NOD. Gravity data were provided with permission from the Norwegian Geological Survey (NGU). Seismic surfaces and modelling files are available upon reasonable request to the corresponding author.

Acknowledgements

This research was funded by the *Akademia* program between Equinor and UiT The Arctic University of Norway. A.P.E.L. acknowledges grants from the European Union's Horizon Europe through Marie Sklodowska-Curie Actions (grant no. 101102324) and from the Research Council of Norway (grant no. 349791). This project has also received funding from the Research Council of Norway through the Centres of Excellence funding scheme, project number 332523 (Centre for Planetary Habitability - PHAB). We thank TGS for allowing us to publish the seismic images and the Norwegian Geological Survey (NGU) for the gravity map. We acknowledge the Kontinentalsokkelundersøkelser (IKU) or Institute for Continental Shelf Investigations, now Stiftelsen for Industriell og Teknisk Forskning (SINTEF), or Foundation for Industrial and Technical Research on behalf of the Norwegian Petroleum Directorate (NPD), now called the Norwegian Offshore Directorate (NOD) for the permission to publish the core data (7517/12-U-01 and 7418/01-U-01). BeicipFranlab and SLB are acknowledged for DionisosFlow and Petrel software under educational licenses to UiT The Arctic University of Norway and Royal Holloway University of London, UK. Perceptually uniform colour maps of Crameri (2018) were used in this paper to avoid visual distortion of the data. We are grateful to the Editor-in-Chief Michele Rebesco and the Reviewers (Wolfram Geissler and two anonymous reviewers) for their detailed and helpful comments that improved the quality of an earlier version of the manuscript.

Appendix A. Supplementary data

Supplementary data to this article can be found online at https://doi.org/10.1016/j.margeo.2024.107447.

References

Backman, J., Jakobsson, M., Frank, M., Sangiorgi, F., Brinkhuis, H., Stickley, C., O'Regan, M., Løvlie, R., Pälike, H., Spofforth, D., 2008. Age model and core-seismic integration for the Cenozoic Arctic Coring Expedition sediments from the Lomonosov Ridge. Paleoceanography 23 (1).

Barabasch, J., Ducros, M., Hawie, N., Daher, S.B., Nader, F.H., Littke, R., 2019. Integrated 3D forward stratigraphic and petroleum system modeling of the Levant Basin, Eastern Mediterranean. Basin Res. 31 (2), 228–252.

Barke, J., van der Burgh, J., Konijnenburg-van Cittert, J.H., Collinson, M.E., Pearce, M. A., Bujak, J., Heilmann-Clausen, C., Speelman, E.N., van Kempen, M.M., Reichart, G.-J., 2012. Coeval Eocene blooms of the freshwater fern Azolla in and around Arctic and Nordic seas. Palaeogeogr. Palaeoclimatol. Palaeoecol. 337, 108–119.

Bergh, S.G., Braathen, A., Andresen, A., 1997. Interaction of basement-involved and thin-skinned tectonism in the Tertiary fold-thrust belt of Central Spitsbergen, Svalbard. AAPG Bull. 81 (4), 637–661.

Berndt, C., Planke, S., Alvarez Zarikian, C.A., Frieling, J., Jones, M.T., Millett, J.M., Brinkhuis, H., Bünz, S., Svensen, H.H., Longman, J., 2023. Shallow-water hydrothermal venting linked to the Palaeocene–Eocene Thermal Maximum. Nat. Geosci. 16 (9), 803–809.

Brinkhuis, H., Schouten, S., Collinson, M.E., Sluijs, A., Damsté, J.S.S., Dickens, G.R., Huber, M., Cronin, T.M., Onodera, J., Takahashi, K., 2006. Episodic fresh surface waters in the Eocene Arctic Ocean. Nature 441 (7093), 606–609.

Burton, Z.F., McHargue, T., Kremer, C.H., Bloch, R.B., Gooley, J.T., Jaikla, C., Harrington, J., Graham, S.A., 2023. Peak Cenozoic warmth enabled deep-sea sand deposition. Sci. Rep. 13 (1), 1276.

Coakley, B., Brumley, K., Lebedeva-Ivanova, N., Mosher, D., 2016. Exploring the geology of the Central Arctic Ocean; understanding the basin features in place and time. J. Geol. Soc. Lond. 173 (6), 967–987.

Colombera, L., Mountney, N.P., 2020. On the geological significance of clastic parasequences. Earth Sci. Rev. 201, 103062.

Crameri, F., 2018. Geodynamic diagnostics, scientific visualisation and StagLab 3.0. Geosci. Model Dev. 11 (6), 2541–2562.

Doré, A., Lundin, E., Gibbons, A., Sømme, T., Tørudbakken, B., 2016. Transform margins of the Arctic: a synthesis and re-evaluation. Geol. Soc. Lond. Spec. Publ. 431 (1), 63–94.

Dumais, M.A., Gernigon, L., Olesen, O., Lim, A., Johansen, S., Brönner, M., 2022. Crustal and thermal heterogeneities across the Fram Strait and the Svalbard margin. Tectonics 41 (10) (e2022TC007302).

Dypvik, H., Riber, L., Burca, F., Rüther, D., Jargvoll, D., Nagy, J., Jochmann, M., 2011. The Paleocene–Eocene thermal maximum (PETM) in Svalbard—clay mineral and geochemical signals. Palaeogeogr. Palaeoclimatol. Palaeoecol. 302 (3–4), 156–169.

Eidvin, T., Jansen, E., Riis, F., 1993. Chronology of Tertiary fan deposits off the western Barents Sea: Implications for the uplift and erosion history of the Barents Shelf. Mar. Geol. 112 (1–4), 109–131.

Eidvin, T., Riis, F., Brekke, H., Smelror, M., 2022. A revised lithostratigraphic scheme for the Eocene to Pleistocene succession on the Norwegian continental shelf. Nor. J. Geol. 1, 1–132.

Eikelmann, I.E.S., 2017. Shallow Stratigraphic Cores NW of Bjørnøya, Results and Implications. UiT Norges Arktiske Univ (M.Sc. Thesis).

Engen, Ø., Faleide, J.I., Dyreng, T.K., 2008. Opening of the Fram Strait gateway: a review of plate tectonic constraints. Tectonophysics 450 (1), 51–69.

Equinor, 2023. Internal Equinor Report.

Evangelatos, J., Mosher, D.C., 2016. Seismic stratigraphy, structure and morphology of Makarov Basin and surrounding regions: tectonic implications. Mar. Geol. 374, 1–13.

Faleide, J.I., Tsikalas, F., Breivik, A.J., Mjelde, R., Ritzmann, O., Engen, Ø., et al., 2008. Structure and evolution of the continental margin off Norway and the Barents Sea. Episodes J. Int. Geosci. 31 (1), 82–91.

Faleide, J.I., Vågnes, E., Gudlaugsson, S.T., 1993. Late Mesozoic-Cenozoic evolution of the South-Western Barents Sea in a regional rift-shear tectonic setting. Mar. Pet. Geol. 10 (3), 186–214.

Faleide, J.I., Bjørlykke, K., Gabrielsen, R.H., 2015. Geology of the Norwegian continental shelf. In: Bjørlykke, K. (Ed.), Petroleum Geoscience: From Sedimentary Environments to Rock Physics, pp. 603–637.

Flowerdew, M.J., Fleming, E.J., Chew, D.M., Morton, A.C., Frei, D., Benedictus, A., Omma, J., Riley, T.R., Badenszki, E., Whitehouse, M.J., 2023. The Importance of Eurekan Mountains on Cenozoic Sediment Routing on the Western Barents Shelf. Geosciences 13 (3), 91.

Foreman, B.Z., Heller, P.L., Clementz, M.T., 2012. Fluvial response to abrupt global warming at the Palaeocene/Eocene boundary. Nature 491 (7422), 92–95.

Gabrielsen, R.H., Faerseth, R.B., Jensen, L.N., 1990. Structural elements of the Norwegian Continental Shelf. Pt. 1. The Barents Sea Region. Norw. Petrol. Direct. Bull. 6.

GEBCO, 2022. GEBCO_2022 Grid.

Granjeon, D., Joseph, P., 1999. Concepts and Applications of a 3-D Multiple Lithology, Diffusive Model in Stratigraphic Modeling.

Green, P., Duddy, I., 2010. Synchronous exhumation events around the Arctic including examples from Barents Sea and Alaska North Slope. In: Geological Society of London, Petroleum Geology Conference Series, 7, pp. 633–644.

Greenwood, D.R., Basinger, J.F., Smith, R.Y., 2010. How wet was the Arctic Eocene rain forest? Estimates of precipitation from Paleogene Arctic macrofloras. Geology 38 (1), 15–18.

Grundvåg, S.A., Helland-Hansen, W., Johannessen, E.P., Eggenhuisen, J., Pohl, F., Spychala, Y., 2023. Deep-water sand transfer by hyperpycnal flows, the Eocene of Spitsbergen, Arctic Norway. Sedimentology 70 (7), 2057–2107.

Hawie, N., Deschamps, R., Granjeon, D., Nader, F.H., Gorini, C., Müller, C., Montadert, L., Baudin, F., 2017. Multi-scale constraints of sediment source to sink systems in frontier basins: a forward stratigraphic modelling case study of the Levant region. Basin Res. 29, 418–445.

Hawie, N., Covault, J.A., Dunlap, D., Sylvester, Z., 2018. Slope-fan depositional architecture from high-resolution forward stratigraphic models. Mar. Pet. Geol. 91, 576–585.

Hegewald, A., Jokat, W., 2013. Relative Sea level variations in the Chukchi region-Arctic Ocean-since the late Eocene. Geophys. Res. Lett. 40 (5), 803–807.

Helland-Hansen, W., Grundvåg, S.A., 2021. The Svalbard Eocene-Oligocene (?) Central Basin succession: Sedimentation patterns and controls. Basin Res. 33 (1), 729–753.

Helland-Hansen, W., Steel, R.J., Sømme, T.O., 2012. Shelf genesis revisited. J. Sediment. Res. 82 (3), 133–148.
Helland-Hansen, W., Sømme, T.O., Martinsen, O.J., Lunt, I., Thurmond, J., 2016. Deciphering Earth's natural hourglasses: perspectives on source-to-sink analysis. J. Sediment. Res. 86 (9), 1008–1033.
Hernández-Molina, F., Llave, E., Stow, D., 2008. Continental slope contourites. Dev. Sedimentol. 60, 379–408.
Hovikoski, J., Fyhn, M.B.W., Nøhr-Hansen, H., Hopper, J.R., Andrews, S., Barham, M., Nielsen, L.H., Bjerager, M., Bojesen-Koefoed, J., Lode, S., Sheldon, E., Uchman, A., Skorstengaard, P.R., Alsen, P., 2021. Paleocene-Eocene volcanic segmentation of the Norwegian-Greenland seaway reorganized high-latitude ocean circulation. Commun. Earth Environ. 2 (1), 172.
Jahren, A.H., Sternberg, L.S.L., 2003. Humidity estimate for the middle Eocene Arctic rain forest. Geology 31 (5), 463–466.
Jahren, A.H., Sternberg, L.S., 2008. Annual patterns within tree rings of the Arctic middle Eocene (ca. 45 Ma): Isotopic signatures of precipitation, relative humidity, and deciduousness. Geology 36 (2), 99–102.
Jakobsson, M., Backman, J., Rudels, B., Nycander, J., Frank, M., Mayer, L., Jokat, W., Sangiorgi, F., O'Regan, M., Brinkhuis, H., 2007. The early Miocene onset of a ventilated circulation regime in the Arctic Ocean. Nature 447 (7147), 986–990.
Japsen, P., Chalmers, J.A., 2000. Neogene Uplift and Tectonics Around the North Atlantic: Overview, 24(3–4), pp. 165–173.
Japsen, P., Green, P.F., Bonow, J.M., Nielsen, T.F., Chalmers, J.A., 2014. From volcanic plains to glaciated peaks: Burial, uplift and exhumation history of southern East Greenland after opening of the NE Atlantic. Glob. Planet. Chang. 116, 91–114.
Japsen, P., Green, P.F., Chalmers, J.A., 2023. Synchronous exhumation episodes across Arctic Canada, North Greenland and Svalbard in relation to the Eurekan Orogeny. Gondwana Res. 117, 207–229.
Jones, M.T., Stokke, E.W., Rooney, A.D., Frieling, J., Pogge von Strandmann, P.A., Wilson, D.J., Svensen, H.H., Planke, S., Adatte, T., Thibault, N., 2023. Tracing North Atlantic volcanism and seaway connectivity across the paleocene–eocene thermal maximum (PETM). Clim. Past 19 (8), 1623–1652.
Kristensen, T.B., Rotevatn, A., Marvik, M., Henstra, G.A., Gawthorpe, R.L., Ravnås, R., 2018. Structural evolution of sheared margin basins: the role of strain partitioning. Sørvestsnaget Basin, Norwegian Barents Sea. Basin Res. 30 (2), 279–301.
Lasabuda, A.P.E., 2013. 3D Seismic Geomorphology of Submarine Channel-Levee Systems in Salt-Related Slope Setting: A Case Study from the Western Deepwater Egypt, Universitetet I Bergen (UiB).
Lasabuda, A., Laberg, J.S., Knutsen, S.-M., Høgseth, G., 2018a. Early to middle Cenozoic paleoenvironment and erosion estimates of the southwestern Barents Sea: Insights from a regional mass-balance approach. Mar. Pet. Geol. 96, 501–521.
Lasabuda, A., Laberg, J.S., Knutsen, S.-M., Safronova, P., 2018b. Cenozoic tectonostratigraphy and pre-glacial erosion: a mass-balance study of the northwestern Barents Sea margin, Norwegian Arctic. J. Geodyn. 119, 149–166.
Lasabuda, A.P., Johansen, N.S., Laberg, J.S., Faleide, J.I., Senger, K., Rydningen, T.A., Patton, H., Knutsen, S.-M., Hanssen, A., 2021. Cenozoic uplift and erosion of the Norwegian Barents Shelf–a review. Earth Sci. Rev. 217, 103609.
Lasabuda, A.P.E., Hanssen, A., Laberg, J.S., Faleide, J.I., Patton, H., Abdelmalak, M.M., Rydningen, T.A., Kjølhamar, B.E., 2023. Paleobathymetric reconstructions of the SW Barents Seaway and their implications for Atlantic-Arctic Ocean circulation. Commun. Earth Environ. 4, 231.
Lasabuda, A.P., Chiarella, D., Sømme, T.O., Grundvåg, S.A., Doré, A.G., Primadani, G., Rydningen, T.A., Laberg, J.S., Hanssen, A., 2024. Unravelling controls on multi-source-to-sink systems: a stratigraphic forward model of the early–middle Cenozoic of the SW Barents Sea. Basin Res. 36 (4), e12883.
Lyck, J.M., Stemmerik, L., 2000. Palynology and depositional history of the Paleocene? Thyra Ø Formation, Wandel Sea Basin, eastern North Greenland. Geol. Greenl. Surv. Bull. 187, 21–49.
McNeil, D., Parsons, M., 2013. The Paleocene-Eocene thermal maximum in the Arctic Beaufort–Mackenzie Basin—Palynomorphs, carbon isotopes and benthic foraminiferal turnover. Bull. Can. Petrol. Geol. 61 (2), 157–186.
Miller, K.G., Kominz, M.A., Browning, J.V., Wright, J.D., Mountain, G.S., Katz, M.E., Sugarman, P.J., Cramer, B.S., Christie-Blick, N., Pekar, S.F., 2005. The Phanerozoic record of global sea-level change. Science 310 (5752), 1293–1298.
Miller, K.G., Browning, J.V., Schmelz, W.J., Kopp, R.E., Mountain, G.S., Wright, J.D., 2020. Cenozoic Sea-level and cryospheric evolution from deep-sea geochemical and continental margin records. Sci. Adv. 6 (20), eaaz1346.
Mitchell, W.H., Whittaker, A.C., Mayall, M., Lonergan, L., Pizzi, M., 2021. Quantifying the relationship between structural deformation and the morphology of submarine channels on the Niger Delta continental slope. Basin Res. 33 (1), 186–209.
Moran, K., Backman, J., Brinkhuis, H., Clemens, S.C., Cronin, T., Dickens, G.R., Eynaud, F., Gattacceca, J., Jakobsson, M., Jordan, R.W., 2006. The cenozoic palaeoenvironment of the arctic ocean. Nature 441 (7093), 601–605.
Mosher, D.C., Shimeld, J., Hutchinson, D., Chian, D., Lebedova-Ivanova, N., Jackson, R., 2012. Canada Basin Revealed, OTC Arctic Technology Conference. OTC (pp. OTC-23797-MS).
Müller, R.D., Zahirovic, S., Williams, S.E., Cannon, J., Seton, M., Bower, D.J., Tetley, M. G., Heine, C., Le Breton, E., Liu, S., 2019. A global plate model including lithospheric deformation along major rifts and orogens since the Triassic. Tectonics 38 (6), 1884–1907.
NPD, 2023. https://factpages.npd.no/en/wellbore/PageView/Exploration/All/4129.
Omosanya, K., Johansen, S., Abrahamson, P., 2016. Magmatic activity during the breakup of Greenland-Eurasia and fluid-flow in Stappen High, SW Barents Sea. Mar. Pet. Geol. 76, 397–411.
Patton, H., Alexandropoulou, N., Lasabuda, A.P., Knies, J., Andreassen, K., Winsborrow, M., Laberg, J.S., Hubbard, A., 2024. Glacial erosion and Quaternary landscape development of the Eurasian Arctic. Earth Sci. Rev. 104936.
Petersen, T.G., 2021. New sequence stratigraphic framework on a 'passive'margin: implications for the post-break-up depositional environment and onset of glaciomarine conditions in NE Greenland. J. Geol. Soc. Lond. 178 (2).
Piepjohn, K., von Gosen, W., Tessensohn, F., 2016. The Eurekan deformation in the Arctic: an outline. J. Geol. Soc. Lond. 173 (6), 1007–1024.
Pirmez, C., Imran, J., 2003. Reconstruction of turbidity currents in Amazon Channel. Mar. Pet. Geol. 20 (6–8), 823–849.
Posamentier, H.W., Kolla, V., 2003. Seismic geomorphology and stratigraphy of depositional elements in deep-water settings. J. Sediment. Res. 73 (3), 367–388.
Rebesco, M., Hernández-Molina, F.J., Van Rooij, D., Wåhlin, A., 2014. Contourites and associated sediments controlled by deep-water circulation processes: state-of-the-art and future considerations. Mar. Geol. 352, 111–154.
Ricketts, B.D., Stephenson, R.A., 1994. The demise of Sverdrup Basin; late Cretaceous-Paleogene sequence stratigraphy and forward modeling. J. Sediment. Res. 64 (4b), 516–530.
Röhl, U., Westerhold, T., Bralower, T.J., Zachos, J.C., 2007. On the duration of the Paleocene-Eocene thermal maximum (PETM). Geochem. Geophys. Geosyst. 8 (12).
Ryseth, A., Augustson, J.H., Charnock, M., Haugerud, O., Knutsen, S.-M., Midbøe, P.S., Opsal, J.G., Sundsbø, G., 2003. Cenozoic stratigraphy and evolution of the Sørvestsnaget Basin, southwestern Barents Sea. Nor. J. Geol. 83 (2), 107–130.
Sættem, J., Bugge, T., Fanavoll, S., Goll, R., Mørk, A., Mørk, M., Smelror, M., Verdenius, J., 1994. Cenozoic margin development and erosion of the Barents Sea: Core evidence from southwest of Bjørnøya. Mar. Geol. 118 (3), 257–281.
Safronova, P.A., Andreassen, K., Laberg, J.S., Vorren, T.O., 2012. Development and post-depositional deformation of a Middle Eocene deep-water sandy depositional system in the Sørvestsnaget Basin, SW Barents Sea. Mar. Pet. Geol. 36 (1), 83–99.
Safronova, P.A., Henriksen, S., Andreassen, K., Laberg, J.S., Vorren, T.O., 2014. Evolution of shelf-margin clinoforms and deep-water fans during the middle Eocene in Sorvestsnaget Basin. AAPG Bull. 98 (3), 515–544.
Sangster, C., Piper, D.J., Hawie, N., Pe-Piper, G., Saint-Ange, F., 2019. Forward stratigraphic modelling of sediment pathways and depocentres in salt-influenced passive-margin basins: lower cretaceous, central Scotian Basin. Basin Res. 31 (4), 728–753.
Sheriff, R.E., 1975. Factors affecting seismic amplitudes. Geophys. Prospect. 23 (1), 125–138.
Sluijs, A., Brinkhuis, H., 2009. A dynamic climate and ecosystem state during the Paleocene-Eocene thermal Maximum: inferences from dinoflagellate cyst assemblages on the New Jersey Shelf. Biogeosciences 6 (8), 1755–1781.
Sluijs, A., Schouten, S., Donders, T.H., Schoon, P.L., Röhl, U., Reichart, G.-J., Sangiorgi, F., Kim, J.-H., Sinninghe Damsté, J.S., Brinkhuis, H., 2009. Warm and wet conditions in the Arctic region during Eocene thermal Maximum 2. Nat. Geosci. 2 (11), 777–780.
Smelror, M., Petrov, O., Larssen, G.B., Werner, S., 2009. Geological history of the Barents Sea. Norges Geol. Undersøkelse 1–135.
Sømme, T.O., Skogseid, J., Embry, P., Løseth, H., 2019. Manifestation of tectonic and climatic perturbations in deep-time stratigraphy–an example from the Paleocene succession offshore western Norway. Front. Earth Sci. 7, 303.
Sømme, T.O., Huwe, S.I., Martinsen, O.J., Sandbakken, P.T., Skogseid, J., Valore, L.A., 2023. Stratigraphic expression of the Paleocene-Eocene thermal Maximum climate event during long-lived transient uplift—an example from a shallow to deep-marine clastic system in the Norwegian Sea. Front. Earth Sci. 11, 1082203.
Stap, L., Lourens, L.J., Thomas, E., Sluijs, A., Bohaty, S., Zachos, J.C., 2010. High-resolution deep-sea carbon and oxygen isotope records of Eocene thermal Maximum 2 and H2. Geology 38 (7), 607–610.
Steel, R., Olsen, T., 2002. Clinoforms, Clinoform Trajectories and Deepwater Sands.
Svensen, H., Planke, S., Malthe-Sørenssen, A., Jamtveit, B., Myklebust, R., Rasmussen Eidem, T., Rey, S.S., 2004. Release of methane from a volcanic basin as a mechanism for initial Eocene global warming. Nature 429 (6991), 542–545.
Svensen, H.H., Bjærke, M.R., Kverndokk, K., 2019. The past as a mirror: deep time climate change exemplarity in the anthropocene. Culture Unbound 11 (3–4), 330–352.
Taner, M.T., Sheriff, R.E., 1977. Application of amplitude, frequency, and other attributes to stratigraphic and hydrocarbon determination: section 2. In: Application of Seismic Reflection Configuration to Stratigraphic Interpretation.
Thomas, E., Boscolo-Galazzo, F., Balestra, B., Monechi, S., Donner, B., Röhl, U., 2018. Early Eocene thermal maximum 3: Biotic response at Walvis Ridge (SE Atlantic Ocean). Paleoceanogr. Paleoclimatol. 33 (8), 862–883.
Tucker, G.E., Slingerland, R.L., 1994. Erosional dynamics, flexural isostasy, and long-lived escarpments: a numerical modeling study. J. Geophys. Res. Solid Earth 99 (B6), 12229–12243.
Westerhold, T., Röhl, U., Laskar, J., Raffi, I., Bowles, J., Lourens, L.J., Zachos, J.C., 2007. On the duration of magnetochrons C24r and C25n and the timing of early Eocene global warming events: Implications from the Ocean Drilling Program Leg 208 Walvis Ridge depth transect. Paleoceanography 22 (2).
Westerhold, T., Röhl, U., Donner, B., Zachos, J.C., 2018. Global extent of early Eocene hyperthermal events: a new Pacific benthic foraminiferal isotope record from Shatsky rise (ODP Site 1209). Paleoceanogr. Paleoclimatol. 33 (6), 626–642.
Westerhold, T., Marwan, N., Drury, A.J., Liebrand, D., Agnini, C., Anagnostou, E., Barnet, J.S., Bohaty, S.M., De Vleeschouwer, D., Florindo, F., 2020. An astronomically dated record of Earth's climate and its predictability over the last 66 million years. Science 369 (6509), 1383–1387.

Wilkinson, C.M., Ganerød, M., Hendriks, B.W., Eide, E.A., 2017. Compilation and appraisal of geochronological data from the North Atlantic Igneous Province (NAIP). Geol. Soc. Lond. Spec. Publ. 447 (1), 69–103.

Zachos, J., Pagani, M., Sloan, L., Thomas, E., Billups, K., 2001. Trends, rhythms, and aberrations in global climate 65 Ma to present. Science 292 (5517), 686–693.

Zachos, J.C., Dickens, G.R., Zeebe, R.E., 2008. An early Cenozoic perspective on greenhouse warming and carbon-cycle dynamics. Nature 451 (7176), 279–283.